This postprint corresponds to the accepted version of a paper published in *The International Journal of Life Cycle Assessment* on 31 March 2026. The published version of the paper is available at https://doi.org/10.1007/s11367-026-02597-1

A parametric life-cycle model for assessing environmental impacts of 4G and 5G cellular base stations

Louis Golard*, louis.golard@uclouvain.be
Robin Dethienne*, robin.dethienne@uclouvain.be
Jérôme Louveaux*, jerome.louveaux@uclouvain.be
David Bol*, david.bol@uclouvain.be

*ICTEAM – UCLouvain, Louvain-la-Neuve, Belgium

Abstract

Purpose This paper presents a parametric life-cycle model to assess the environmental impacts of up-to-date commercial 4G and 5G cellular base stations. While most existing studies emphasize operational energy consumption, the proposed model covers all life-cycle stages with a focus on the production stage. It is intended to support eco-design of base stations and optimize deployment strategies of radio access networks as they rapidly evolve to cope with the dramatic growth in mobile data traffic.

Methods The proposed model is configurable according to variables representing features controlled by network operators and operating conditions imposed by users. It follows a generic functional unit: the provision of wireless communication service(s). The parametric modules of the model differentiate between base station components and life-cycle stages, comprising multiple foreground processes. The corresponding impact assessment factors are calculated from background modeling using ecoinvent 3.10 with the multi-indicator method Environmental Footprint 3.1. Approximate numerical model parameters are obtained from regression analyses based on detailed component teardowns, manufacturer technical documentation and network operator information, thereby enabling quantitative comparisons between base station configurations. Furthermore, uncertainty in the model and numerical estimates is quantified by estimating variability of regressions and by assessing modeling errors.

Results and discussion Life cycle assessment results are obtained by applying the model to six typical base station configurations. Among all impact indicators, the results show that energy consumption in the use stage accounts for 80% to >95% of total global warming potential, and that the production stage is the second largest contributor with a range of 1000 to 4000 kg CO_2 eq per base station. Conversely, the use of mineral and metal resources is more balanced between the production and use stages. Although macro base stations have a greater impact per unit than micro base stations, they also have greater coverage and capacity, which benefits their impact per communication service provided. Moreover, uncertainty analysis shows an interquartile range of ±20% with respect to the median of stochastic assessments.

Conclusions Thanks to its flexibility, the proposed model helps to identify trade-offs in mobile network configuration to provide capacity and coverage with minimum environmental impact. Given the dominant contribution of the use stage, reducing the carbon intensity of the electricity consumed by base stations is critical to reducing their global warming potential. However, it is equally important to consider the production stage if the goal is to reduce the use of mineral and metal resources.

Keywords

Base station – Radio access network – 4G-LTE – 5G-NR – Life cycle assessment – Parametric life-cycle model – Teardown – Uncertainty analysis

Table of Contents

1 Introduction

The rapid expansion of information and communication technologies (ICTs) has driven the intensive development of mobile communication networks that connect mobile terminals to the Internet. On a global scale, Malmodin et al. (2024) estimate that these networks consumed about 161 TWh of electricity and emitted 118 Mt CO_2 eq in 2020, with the largest share attributable to radio access networks (RANs). A RAN comprises numerous base stations (BSs) that transmit and receive radio signals to and from mobile terminals to establish connections with the mobile core network. Historical data show that the energy and carbon footprints of RANs have increased continuously over time (Malmodin and Lundén 2018; Lundén et al. 2022; Malmodin et al. 2024), and country-level forecasts predict that they will continue to increase in the future (Bieser et al. 2020; Golard et al. 2023; Stobbe et al. 2023). These alarming findings call for a paradigm shift in the mobile network industry to meet the greenhouse gas (GHG) reduction target of -36% between 2020 and 2030, as set by the International Telecommunication Union (ITU) in line with the Paris Agreement (ITU-T L.1470 2020).

Informed decision-making is essential for the design and deployment of more sustainable mobile networks. However, most studies to date aimed at modeling and optimizing RANs have focused on the energy consumption of BSs during their use stage, assuming that this is the hotspot in terms of environmental impacts compared to the other life-cycle stages. Although this assumption may hold true for the climate change indicator (Scharnhorst 2008; Malmodin et al. 2014), it has not yet been rigorously verified for other environmental impact indicators through a multi-criteria life cycle assessment (LCA). Recent trends in the sector also suggest that the contribution of the production stage may become significant in the future. Due to the rapid growth of mobile data traffic (Lundén et al. 2022; Ericsson 2024), mobile network operators (MNOs) are seeking to provide more capacity to their subscribers. For instance, MNOs tend to install additional frequency bands on existing BSs and deploy new high-capacity BSs. The latter operate at lower power levels and cover smaller areas, enabling RAN densification (Humar et al. 2011; Tombaz et al. 2011). Thus, new up-to-date equipment must be manufactured. The ensuing acceleration in the pace of technological development is also likely to shorten BS lifetimes due to technical obsolescence (Santarius et al. 2022). Additionally, the greater use of renewable energy sources to operate the RAN (Lundén et al. 2022) tends to reduce the relative contribution of the use stage for several environmental impact indicators (e.g., climate change), but it may also shift the burden to other indicators and life-cycle stages. Conversely, the use of recycled materials could reduce the need for raw material extraction and hence reduce the impacts of BS production (Scharnhorst et al. 2006a). This points out the need for a better understanding of the environmental impacts associated with the full life cycle of BSs, and in particular their production.

1.1 State of the art

In the literature, the electrical energy consumption of various types of BSs is extensively studied using parametric power models, which are useful for assessing impacts during the use stage. Single-band traditional BSs are analyzed by Jung et al. (2014), Debaillie et al. (2015), and Wang et al. (2017), while multi-band BSs are studied by Lorincz and Matijevic (2014). More advanced systems, such as BSs equipped with massive multiple-input multiple-output (MIMO), are modeled by Desset et al. (2014) and Björnson et al. (2015), and mmWave and THz systems are explored by Desset et al. (2020). These models evaluate both the static and dynamic power consumption of BSs as a function of their traffic load. Our recent study (Golard et al. 2024) builds on these previous works to propose an up-to-date parametric power model with realistic numerical parameters estimated by combining on-site measurements with radio equipment documentation. However, looking at power consumption alone is not sufficient to assess the full environmental impacts of the life cycle of a BS. For instance, Humar et al. (2011) demonstrate that the energy-optimal RAN deployment strategy shifts significantly when embodied energy is included in the optimization problem.

While the environmental impacts of the use stage can be easily assessed based on the energy consumption of BSs, those of the other life-cycle stages are much less studied in the literature. Moreover, the focus is mainly, if not exclusively, on the climate change impact category. Initial research efforts by Scharnhorst et al. (2005), Scharnhorst et al. (2006a) and Faist Emmenegger et al. (2006) estimate that the production of 2G-GSM and 3G-UMTS RANs represents between 0.02 and 20 kg CO_2 eq per Gbit of data transmitted. This wide range of results is largely due to the "per Gbit" functional unit (FU), which is highly sensitive to the assumed performance and lifetime of the system. Based on a different FU, Malmodin et al. (2014) assess the carbon footprint of producing similar RANs at 3.5 kg CO_2 eq per subscription per year. Later, Bergmark (2015) estimates 4000 kg CO_2 eq for the production of one BS supporting 4G-LTE, which, according to their assumptions, corresponds to 0.5 kg CO_2 eq per subscription per year. For 5G-NR BSs, Bieser et al. (2020), Ding et al. (2022), Stobbe et al. (2023) and Aubet et al. (2024) provide preliminary LCA results ranging from 3000 kg CO_2 eq for producing a single-band BS to over 10000 kg CO_2 eq for a more advanced multi-band BS. It is worth noting that other studies such as Madon (2021), Kallio et al. (2021) and Guérid et al. (2022) focus on specific components of modern BSs.

When it comes to comparing or combining these works, a first issue is the significant difference in their scope, e.g., some include the construction of concrete terrace and antenna tower while others focus solely on communication-specific equipment. Excluding construction activities, all studies show that most impacts of the production stage come from the manufacturing of electronic components, especially integrated circuits (ICs), and from aluminum production, mainly used in BS component casings. Another issue is the use of different FUs, e.g., some LCA studies assess the impacts of an entire BS, while others normalize their results per bit of transferred data or per subscription. A tentative harmonization of the results indicates that estimates of the embodied carbon footprint vary by an order of magnitude, from 3000 to over 30000 kg CO_2 eq per BS. Using the power model of Golard et al. (2024), this can be compared to the use stage of a typical single-band macro BS, which consumes on average about 2 kW and thus emits 5800 kg CO_2 eq per year of operation, assuming the average electricity grid mix in Europe (Scarlat et al. 2022). Besides, a common limitation in previous studies is the reliance on generic background processes from LCA databases as proxies for BS components due to a lack of specific teardown data, as also pointed out by Bordage et al. (2021), Golard et al. (2023), Stobbe et al. (2023) and Aubet et al. (2024). The last main limitation is that all previous LCA studies evaluate fixed BS configurations without offering parametric life-cycle models that could be used, e.g., to optimize RANs and support deployment strategy planning.

1.2 Contributions

This paper introduces a parametric life-cycle model of an entire BS to assess in detail its environmental impacts across multiple indicators and over its full life cycle. It covers up-to-date commercial BS architectures for outdoor RANs, i.e., large-scale (macro and micro) cellular BSs that emit from one to hundreds of watts per cell and support multiple sub-6 GHz frequency bands using 4G-LTE and 5G-NR communication protocols. However, small-scale BSs, such as pico and femto BSs emitting up to 1 W per cell, are excluded as they are not primarily intended for deployment at sub-6 GHz and are better suited to indoor enterprise and private networks (Lehr et al. 2021). This model aims to support future works on the eco-design and optimization of next-generation BSs as it helps, e.g., to identify the most environmentally optimal BS configuration with respect to network requirements in terms of coverage, capacity, energy consumption, etc. It can also be used in broader studies such as country-level RAN evaluations like Bieser et al. (2020), Golard et al. (2023), Stobbe et al. (2023) and Aubet et al. (2024).

We apply the attributional LCA methodology with a primary focus on the production stage (i.e., a cradle-to-gate LCA), as the modeling of this stage is still rather vague in the literature, even though we also model the distribution, use, and end-of-life stages. Our innovative modular and parametric modeling strategy ensures that the LCA model is highly flexible and can be used to study a wide range of BSs according to their feature configuration. This is particularly useful given the complexity and heterogeneity of the product system. It also allows for a detailed breakdown of impacts by life-cycle stage and by BS component. In addition, we provide approximate yet realistic numerical values for the model parameters, including environmental impact factors, to enable quantitative comparisons between different BS configurations. These parameters are estimated from an in-depth analysis of the design and hardware composition of BS components based on specific data sources such as detailed teardowns, manufacturer technical documentation, and information from MNOs. This is another key contribution to filling the gap in specific data on BS components. Finally, we quantify the uncertainties in our model for the purpose of uncertainty and sensitivity analyses of the results.

1.3 Paper structure

This paper is structured as follows. Section 2 outlines the methodology used to develop the model, explaining the LCA modeling strategies and data sources. Section 3 introduces the parametric life-cycle model, first specifying its goal and scope, then detailing the inventory of foreground processes for all BS components, before calculating the corresponding multi-indicator impact factors, and performing the uncertainty quantification. Section 4 applies the proposed model to several BS configurations and interprets examples of results that can be obtained. Finally, Section 5 discusses the limitations of the model and formulates practical recommendations for the users of the model. In addition to this core paper, supplementary information is provided as online resources to detail all modeling assumptions and to fully define the proposed parametric model for use in future works.

2 Methodology

In this work, we use the attributional process-based LCA methodology defined by the ISO 14040 (2006). In addition, we follow the (widely accepted) recommendation ITU-T L.1410 (2014) on how to apply LCA specifically to ICTs in order to allow other researchers to use this model while ensuring consistency. Accordingly, the BS is an *ICT network good* that can be used as a building block to assess the environmental impacts of *ICT networks* and *ICT services*. Figure 1 shows the system boundaries of our LCA based on the processes considered in ITU-T L.1410 (2014). We exclude from the system boundary *support goods* (e.g., antenna support towers, building, monitoring and security equipment, etc.) and some *support activities* (e.g., maintenance, business activities, etc.) because they are either not strictly necessary for the proper operation of the BS or are not applicable because the BS is considered as an ICT good and not as the service provided by the RAN.

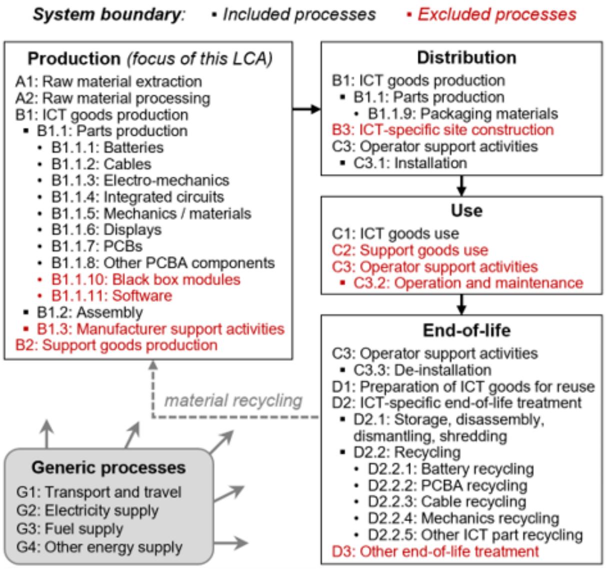

Fig. 1 System boundary for the assessment of a base station according to the recommendation ITU-T L.1410 (2014) with processes grouped into 4 life-cycle stages (slightly adapted from the ITU recommendation)

2.1 Modeling strategies

A cellular BS consists of 5 types of main components: the baseband unit (BBU) for digital baseband functions, the radio unit (RU) for analog baseband and radio-frequency functions plus signal amplification, the antenna unit (AU) for radio-wave transmission and reception, the power supply unit (PSU) for power conversion and distribution, and the cables for connecting all these components. The composition of these components varies according to the BS feature configuration. However, conducting an LCA of such a complex and heterogeneous product system is known to be labor-intensive and time-consuming (Scharnhorst 2008). Therefore, we propose to apply two modeling strategies together to simplify the LCA implementation: the *modular* LCA approach and the *parametric* LCA approach, as proposed by Kiemel et al. (2022).

The modular LCA approach involves modeling the product system around reusable elements called modules. Each specific module is first modeled separately, then aggregated together to constitute the whole system (Kiemel et al. 2022). In our model, we define eight modules: we consider five separate modules for the production of each of the five main BS component, to which we add three modules for the distribution, use and end-of-life stages. The modules representing the production of the BBU, RU, AU and cables can be used multiple times for modeling a single BS (i.e., once for each cell), depending on its configuration. Since we consider multiple impact category indicators, the total impact of a BS is represented by a column vector as

$$I_{BS} = \sum_{m=1}^{M} I_m \ ,$$

where M is the total number of BS modules, and I_m is the impact vector of the module m.

The parametric LCA approach aims to model the product system, or its modules, through a set of product-related parameters. This requires determining the functions linking these parameters to the environmental impacts of the system, which often involves regression analysis (Kiemel et al. 2022). In our model, the impact of each foreground process for a given indicator category is the product of two terms: the quantity of that process and the corresponding impact factor. We assume that these two terms can be modeled by parametric (often non-linear) functions of a set of model variables $x \in X$ that define the BS configuration, and we determine these functions using regression analysis on specific data sources.

The impact of a module m of the LCA model is then computed by adding together the impacts of its K_m foreground processes. Hence, the column vector of all its impacts is

$$I_m(x) = \sum_{k=1}^{K_m} q_k(x) F_k(x) \ ,$$

where $q_k(x)$ is the parametric quantity of the foreground process k for the BS configuration x, and $F_k(x)$ is the vector column of its parametric impact factors. It can be rewritten as a matrix product as

$$I_m(x) = \boldsymbol{F}_m(x) Q_m(x)^T \ ,$$

where $Q_m(x)$ is the row vector of all process quantities in the module, and $\boldsymbol{F}_m(x)$ is the matrix resulting from horizontal concatenation of column vectors $F_k(x)$. Note that the units of the elements in any vector $Q_m(x)$ are those used to scale the corresponding impact factors, and may therefore be different (e.g., kg, km, cm², etc.).

2.2 Model variables

The challenge is then to determine X the set of *model variables* for modeling the parametric BS modules. These variables must represent the service provided by the BS in order for the proposed model to be flexible and easily exploited in future works. For instance, it should represent features that can be configured by MNOs, as well as the operating conditions imposed by network users. As a BS may serve multiple sector and support multiple frequency bands, the first key model variables are the number of sectors N_S and the number of frequency bands N_B. By defining a *cell* as being one frequency band covering one sector, the total number of cells is $N_C = N_S N_B$, e.g., a 3-sectors BS with 2 bands contains 6 cells. Moreover, we identify other key variables that must be defined for each cell such as the carrier frequency, the bandwidth, the maximum output power per transmit chain, the duplex scheme either frequency division duplex (FDD) or time division duplex (TDD), etc. Additional variables are considered for the distribution stage (e.g., the international distribution distance), for the use stage (e.g., the lifetime), and for the end-of-life (e.g., the waste management route). Table 1 provides the complete set of model variables. The number of spatial data layers refers to the maximum number of supported MIMO layers, and the maximum total antenna gain refers to the maximum antenna gain of the whole AU when forming a single beam. We already used a similar set of variables in Golard et al. (2024) for our parametric BS power model.

Table 1 Complete set of model variables

Scope	Description	Symbol	Unit*	Validity range
for the entire base station	number of sectors	N_S	#	1-5
	number of frequency bands	N_B	#	1-7
	duration of backup battery at full load	τ_{back}	hours	0-3
	distance between baseband and antenna units	d_{AU}	m	0-50
	distance of international distribution	d_{inter}	km	0-40000
	distance of local distribution	d_{loc}	km	0-1000
	average load in physical resources**	$\bar{l}_{avg}$	/	0-1
	lifetime	L	years	0-20
	source of electricity consumption	-	n.a.	diesel generator, grid or PV system
	route of waste management	-	n.a.	disposal or recycling
for each cell	carrier frequency	f	GHz	0-6
	bandwidth	B	MHz	5-200
	number of spatial data layers	N_L	#	1-8
	maximum output power per transmit chain	P_{TX}	W	1-80
	maximum total antenna gain	$G_{TX,dB}$	dBi	0-25
	number of transmit chains	N_{TX}	#	1-64
	number of receive chains	N_{RX}	#	1-64
	relative position of radio units between baseband unit and antenna units	δ_{cab}	/	0-1
	duplex scheme	-	n.a.	FDD or TDD
	communication protocol	-	n.a.	4G-LTE or 5G-NR
	adaptive beamforming	-	n.a.	without or with
	type of antenna unit	-	n.a.	traditional or AAU

* "#" = integer number; "/" = without unit; "n.a." = not applicable
** the load can also be defined for each cell as in Golard et al. (2024)

2.3 Regression analysis

The non-linear parametric functions of our model are determined using regression analysis (Rawlings et al. 1998). We define that the independent variables in the regressions are (a subset of) the model variables X (e.g., the number of transmit chains N_{TX}), while the dependent variables are the foreground process quantities (e.g., the total mass of RUs). The behavior of these regression functions is controlled by *model parameters* (e.g., the mass density of the RU casing) that depend on the technology and, unlike model variables, cannot be configured by MNOs nor influenced by users. Denoting θ as the set of model parameters, we can rewrite the kth process quantity function of a BS configuration x as $q_k(x, \theta)$. Then, to compute $\hat{\theta}$, the set of numerical model parameter estimates, we use specific data sources comprising D pieces of equipment from existing BSs (these are our observations) for which we know the feature configurations $\Phi = \{\phi_1, \phi_2 \dots \phi_D\}$ and the actual process quantities $Y = \{y_1, y_2 \dots y_D\}$. Regression model fitting is achieved by solving the non-linear least squares problem

$$\hat{\theta} = \arg\min_{\theta} \left\{ \sum_{d=1}^{D} \left(y_d - q(\phi_d, \theta) \right)^2 \right\}$$

using numerical methods. In Table 1, the validity ranges of model variables delineate the domain of BS configurations within which we consider our numerical estimates (and associated uncertainties) to be valid. These validity ranges are based on the range of equipment configurations available in the specific data sources used for this work. Therefore, the numerical estimates provided in this paper can model BSs whose configurations lie within the validity domain but cannot predict the impacts of BS configurations outside this domain.

2.4 Specific data sources

This LCA study relies on three types of specific data sources: (i) teardowns of BS components, (ii) technical documentation from BS manufacturers, and (iii) data and information from MNOs. These sources are used to determine parametric foreground process models via regression analysis and calculate their specific impact factors. Thus, specific data sources are constructed to represent the full range of BS configurations covered by the scope of this work, which enables consistent validity ranges for model variables (see Table 1).

Teardowns enable to precisely quantify the material composition of BS components as a function of the BS configuration. However, detailed teardowns are time-consuming to perform and require direct access to the components, with permission to degrade them. We first carried out teardowns of a BBU, a remote RU and a traditional passive AU of a macro cellular BS from the 2010's, supporting several frequency bands, including 4G-LTE at 1.8 GHz with 20 MHz bandwidth and two layers. Figure 2 shows pictures of these disassembled components. Detailed pictures of these teardowns are available in Online Resource 1. In addition, we use a dozen additional teardowns from various external sources covering other BS configurations: from legacy 3G BSs to up-to-date 5G BSs with massive-MIMO at 3.5 GHz, as well as micro BSs (see in Online Resource 1).

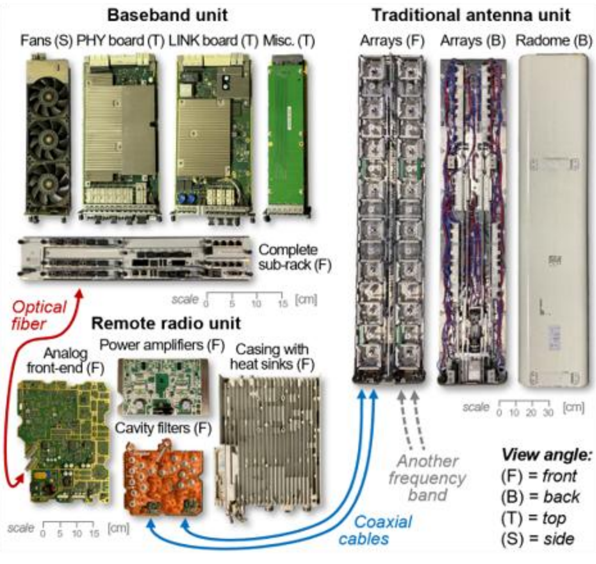

Fig. 2 Pictures of our own teardowns of a baseband unit, a remote radio unit and a traditional passive antenna unit of a macro cellular base station. No teardown of a power supply unit was carried out, and power cables are not shown. Pictures of the different components are not to the same scale

Technical documentation from manufacturers provides a comprehensive description of their BS configuration and related technical specifications. Following recommendations ETSI ES 202 706-1 (2022) and EU 2021/2279 (2021), some manufacturers now provide the dynamic power consumption and bill-of-materials of their products, which is useful for modeling the operating energy consumption, and for complementing the quantification of material composition. In contrast to the teardowns, equipment documentation covers a much wider range of components, with various feature configurations. The drawback of using such secondary data sources is that they sometimes offer less detail than required for in-depth LCA modeling. In this work, we use the documentation of several hundred pieces of equipment provided by MNOs. For confidentiality reasons, the technical documentation cannot be published.

Information and internal data provided by MNOs give additional insight into field practices, especially for installation, operation and de-installation of BSs. Knowledge about specific configurations of all the BSs making up a RAN helps to model how the different BS components are configured in practice. For this work, we obtained information and data on RANs from two main MNOs in Belgium in 2023. Again, it cannot be published for confidentiality reasons.

2.5 Model structure

The general structure of the BS life-cycle model is shown in Figure 3, where we combine the modular and parametric LCA approaches to compute I_{BS}. Within this framework, the environmental impacts of producing the BBU, RUs, AUs and cables are modeled for each cell c by $I_{BBU,c}$, $I_{RU,c}$, $I_{AU,c}$ and $I_{cab,c}$ respectively. These impacts depend on the specific cell configuration defined by the variable subset $X_c \subseteq X$. The impacts of producing the PSU serving all cells of the BS is modeled by I_{PSU}, and the impacts of the distribution, use and end-of-life stages are denoted by I_{dist}, I_{use} and I_{EoL}, respectively. All these terms result from the combination of the *foreground process inventory* (FPI) with corresponding *impact assessment factors* (IAFs). The goal of this distinction is to bring transparency and flexibility to the model, especially for model users who prefer to employ their own IAFs, e.g., for alternative technologies, alternative operating locations, based on impact factors from another database, etc. Therefore, Section 3 deals separately with the FPI and the calculations of IAFs.

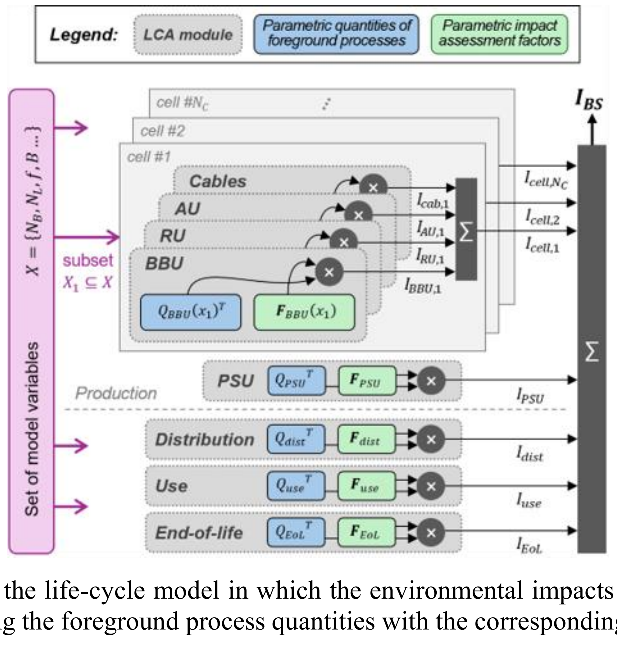

Fig. 3 General structure of the life-cycle model in which the environmental impacts of each parametric module are computed by multiplying the foreground process quantities with the corresponding impact assessment factors

3 Parametric life-cycle model

This section presents the parametric model of the BS life cycle developed according to the methodology described in Section 2. It covers the first three phases of the LCA methodology, namely: (i) the *goal and scope definition*, (ii) the *life-cycle inventory* (LCI) *analysis*, and (iii) the *life-cycle impact assessment* (LCIA). The last part covers the quantification of the uncertainty associated with our modeling and regression analyses.

3.1 Goal and scope

The goal of the proposed BS life-cycle model is to enable researchers, MNOs and network equipment manufacturers to compare the impacts of different BS configurations, to eco-design next-generation BSs, and to support decisions on more sustainable RAN deployment strategies. The product system of the LCA encompasses large-scale multi-band sub-6 GHz cellular BSs for outdoor RANs that supports up to several communication protocols including 4G-LTE and 5G-NR. This range of BSs provides various wireless communication service(s) depending on the BS configuration, in particular Internet access to mobile users who may be human subscribers or connected objects. The system boundaries include the production, distribution, use and end-of-life stages of all communication-specific BS components, and excludes support goods and activities. Core network and backhaul components, data servers and mobile terminals are also excluded from the scope.

The FU is defined as *the provision of given terrestrial wireless communication service(s) by one BS deployed in a given region*. This definition is intentionally generic and non-quantitative, as indicated by the term *given*. This generic approach allows the model to cover the full intended range of BSs and provides more flexibility. Yet, to meet the goal and scope of a specific LCA study, the FU definition can be refined and quantified, e.g., for a quantified time period (e.g., one year), a quantified land area covered (e.g., one km²), a quantified unit of communication service (e.g., one GB of data traffic), a specific region (e.g., in Belgium), etc. Moreover, a given FU can be fulfilled by different BS configurations associated with reference flows defined by the set of model variables $X = \{N_B, N_L, f, B \dots\}$. However, these variables do not fully determine the quality of service provided by a given BS, as it also depends on the signal propagation environment, the network and user density, the traffic load, etc. Nevertheless, in this paper, we focus on modeling BSs solely based on their feature configuration in order not to depend on radio channel models that are specific to each BS site. Figure 4 shows the flow diagram of the product system, highlighting the FU and the reference flows.

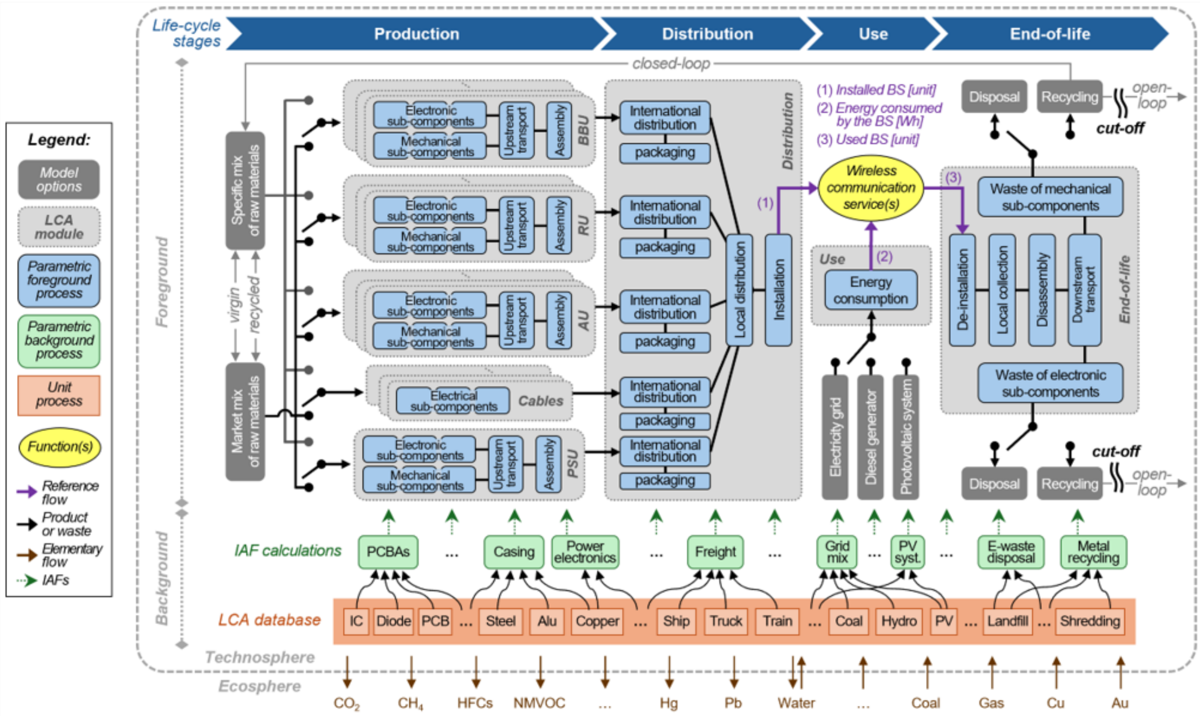

Fig. 4 Flow diagram of the base station life-cycle model divided into: (i) a foreground system combining parametric foreground processes in several life-cycle assessment modules, sometimes depending on specific model options, and (ii) a background system building parametric background processes based on unit processes from a database to calculate impact assessment factors

The LCI analysis involves combining the foreground and background system models (Hauschild et al. 2018). In this paper, we define the *foreground* processes as the main processes of the BS life cycle, for which we seek to establish parametric models. The *background* modeling of these processes consists of informed combination of generic unit processes from the LCA database "ecoinvent version 3.10" (Wernet et al. 2016). Both foreground and background systems are distinguished in Figure 4. The *attributional* modeling perspective is adopted, which implies the use of allocation rules to handle multifunctionality (Hauschild et al. 2018). We therefore use the "allocation, cut-off by classification" system model of ecoinvent (Wernet et al. 2016). The LCIA results are then computed using the multi-indicator LCIA method "Environmental Footprint version 3.1" (EF 3.1) without long-term effects (Andreasi Bassi et al. 2023).

In most cases, no specific allocation procedure is required in the foreground system as most processes deliver separate product flows. One exception relates to freight transportation impacts that are allocated to products based on their mass and the transport distance. In addition, some FU definitions may require special allocation procedures, e.g., when the FU focuses on a specific cell or a specific communication service. Regarding recycling, the allocation of burdens and credits between two successive product life cycles follows the same approach as the ecoinvent cut-off model: no benefits from recycling are allocated to the first life cycle and all burdens due to the recycling process are attributed to the use of recycled materials in the second life cycle (Wernet et al. 2016). As depicted in Figure 4, the open-loop recycling processes are cut off once subcomponent waste leaves the product system at the end-of-life stage. Yet, impacts of recycling processes are embedded in the recycled raw materials at the production stage. For closed-loop recycling, the cut-off approach does not affect the total impacts of the BS life cycle. Rather, it states that the impacts of recycling are counted at the production stage and not at the end-of-life stage.

Table 2 Foreground process inventory

Scope	Module	Description	Parametric functions*	Unit
for each cell	production of the baseband unit	production of the link-layer boards	$e_{link}(x_c)$	cm²
for each cell	production of the baseband unit	production of the physical-layer boards	$e_{phy}(x_c)$	cm²
for each cell	production of the baseband unit	production of the miscellaneous electronics	$e_{misc}(x_c)$	cm²
for each cell	production of the baseband unit	production of the mechanical structure	$m_{BBU}(x_c)$	kg
for each cell	production of the baseband unit	upstream transport of the sub-components	$t_{BBU}(x_c)$	kg·km
for each cell	production of the baseband unit	final assembly of the component	$a_{BBU}(x_c)$	Wh
for each cell	production of the radio unit	production of the power supply	$e_{sup}(x_c)$	cm²
for each cell	production of the radio unit	production of the processing units	$e_{proc}(x_c)$	cm²
for each cell	production of the radio unit	production of the transceivers	$e_{TRX}(x_c)$	cm²
for each cell	production of the radio unit	production of the power amplifiers	$e_{PA}(x_c)$	cm²
for each cell	production of the radio unit	production of the mechanical structure	$m_{RU}(x_c)$	kg
for each cell	production of the radio unit	upstream transport of the sub-components	$t_{RU}(x_c)$	kg·km
for each cell	production of the radio unit	final assembly of the component	$a_{RU}(x_c)$	Wh
for each cell	production of the antenna unit	production of the antenna elements	$e_{AE}(x_c)$	kg
for each cell	production of the antenna unit	production of the mechanical structure	$m_{AU}(x_c)$	kg
for each cell	production of the antenna unit	upstream transport of the sub-components	$t_{AU}(x_c)$	kg·km
for each cell	production of the antenna unit	final assembly of the component	$a_{AU}(x_c)$	Wh
for each cell	production of cables	production of the optical cables	$e_{opt}(x_c)$	m
for each cell	production of cables	production of the coaxial cables	$e_{coax}(x_c)$	m
for each cell	production of cables	production of the power cables	$e_{pwr}(x_c)$	m
for the entire base station	production of the power supply unit	production of the power converter	$e_{conv}(x)$	kg
for the entire base station	production of the power supply unit	production of the backup batteries	$e_{batt}(x)$	kg
for the entire base station	production of the power supply unit	production of the mechanical structure	$m_{PSU}(x)$	kg
for the entire base station	production of the power supply unit	upstream transport of the sub-components	$t_{PSU}(x)$	kg·km
for the entire base station	production of the power supply unit	final assembly of the component	$a_{PSU}(x)$	Wh
for the entire base station	distribution stage	production and disposal of the packaging	$m_{pack}(x)$	kg
for the entire base station	distribution stage	international distribution of the main components	$t_{inter}(x)$	kg·km
for the entire base station	distribution stage	local distribution of the base station	$t_{loc}(x)$	km
for the entire base station	distribution stage	installation of the base station	$a_{inst}(x)$	Wh
for the entire base station	use stage	energy consumption of the base station	$\epsilon_{cons}(x)$	Wh
for the entire base station	end-of-life stage	de-installation of the base station	$a_{deinst}(x)$	Wh
for the entire base station	end-of-life stage	local collection of the base station	$t_{col}(x)$	km
for the entire base station	end-of-life stage	disassembly of the base station	$a_{disas}(x)$	Wh
for the entire base station	end-of-life stage	downstream transport of the sub-components	$t_{down}(x)$	kg·km
for the entire base station	end-of-life stage	waste management of the electronic sub-components	$e_{waste}(x)$	kg
for the entire base station	end-of-life stage	waste management of the mechanical sub-components	$m_{waste}(x)$	kg

* the functions of modules defined for each cell depend on the respective subset X_c of model variables

3.2 Foreground process inventory

The FPI consists in determining the parametric functions of the foreground process quantities that constitute the vector $Q(x)$ for each module of the life-cycle model. This section describes all LCA modules of the BS and their respective modeling in parametric foreground processes. The complete set of foreground processes is provided in Table 2 along with the scaling units to be used when multiplying them by the IAFs. As explained in Section 2.1, the modules representing BBU, RU, AU and cable production can be used multiple times for modeling a single BS. The main modeling assumptions as well as the mathematical expression of all parametric functions with associated numerical parameter estimates are provided in Online Resource 1.

3.2.1 Modeling approach for the production

The production stage includes raw material acquisition, manufacturing, transport and assembly. As shown in Figure 4, raw materials can be either virgin or recycled. By default, our model assumes that the weighting between these two sources corresponds to the market mix for each material. Another option, which we condition on the adoption of end-of-life recycling, considers the use of a specific raw material mix that contains more recycled material than the market average. Yet specific mixes are limited to materials that can be recycled in a closed loop within the product system, i.e., the metals in mechanical structures but not the materials in electronic components as they require a very high level of purity (Krishnan et al. 2008). The foreground processes involved in the production of main BS components are grouped into four types: the production of electronic sub-components, the production of mechanical sub-components, the upstream transport of these sub-components from their respective manufacturing factories to the final assembly factory, and the final assembly of the component. In Table 2, we distinguish the four types of process by a specific symbol, respectively e, m, t and a. Notice that these symbols are also used in the other life-cycle stages to identify related processes: t for transport, a for (de-)installation/disassembly, and e and m for waste management of electronic and mechanical sub-components.

To model the production of most sub-components, we scale their quantity according to scaling variables relative to a reference situation. It means that the quantity $q_k(x)$ of a process k is modeled using a reference quantity q_k^{ref} that scales with S scaling variables as

$$q_k(x) = q_k^{ref} \prod_{s=1}^{S} \left(\frac{x_s}{x_s^\star}\right)^{\alpha_{k,s}} ,$$

where the scaling variable s has an actual value x_s, a reference value $x_s^\star$, and a process-specific scaling exponent $\alpha_{k,s}$. We define the reference situation by $f^\star$=1 GHz, $B^\star$=1 MHz, $P^\star$=1 W, $\tau^\star$=1 hour, $\mathcal{M}^\star$=1 kg, and $\mathcal{A}^\star$=1 cm², respectively the reference frequency, bandwidth, power, duration, mass, and surface area. For each foreground process, the model parameters q_k^{ref} and $\alpha_{k,s}$ are estimated using the method explained in Section 2.3. Yet, to simplify calculations, we restrict scaling exponents to specific values $\alpha \in \{0, 0.25, 0.5, 0.75, 1\}$. A similar scaling approach was previously proposed for BS power consumption models in Debaillie et al. (2015) and Golard et al. (2024). Online resource 1 details how regression analyses are performed on the specific data sources and assesses the goodness-of-fit through the root mean squared error (RMSE) and the coefficient of determination (R^2). For instance, the R^2 values for the FPI of production stage modules ranges from 0.29 to 0.98, with a median value of 0.70, supporting the reliability of our models within the validity domain of model variables.

The modeling approach for transport and assembly processes is the same for all BS components. Due to a lack of primary data, assumptions are needed to model these two types of processes, implying a wider range of uncertainty than relying on specific data sources. Upstream transport is modeled by a mix of freight transportation means for the sub-component mass over the upstream transport distance (in kg·km). Here, the packaging is not modeled as we consider its impacts to be negligible. Assembly is limited to the electricity used for assembling the sub-components into the final BS component, and other assembly processes as well as the construction of the assembly factory are neglected due to lack of information. Manufacturer support activities are outside the scope of this work as mentioned in Figure 1.

3.2.2 Production stage modules

In the BS communication chain, the BBU performs digital functions such as physical resource scheduling, coding, modulation, digital precoding and/or beamforming, decoding, demodulation, etc. (Golard et al. 2024). The BBU is usually made up of a set of boards handling the link and physical layers of communication protocols (Larmo et al. 2009) such as 4G-LTE and 5G-NR. In general, link-layer boards are shared by all BS cells, whereas physical layer boards are dedicated to specific cells or bands, as they are usually optimized for a specific protocol. The BBU boards are the electronic sub-components of the BBU, which we model by the surface areas of their printed circuit board assemblies (PCBAs). Since the impacts of BBU production are modeled per cell in the proposed BS life-cycle model, the PCBA area of link-layer boards is first calculated for the entire BS and then allocated per cell. In contrast, the PCBA area of physical-layer boards is modeled directly for each BS cell. An additional area of PCBA is considered for miscellaneous functions such as power management, fan cooling, etc. The mechanical structure of the BBU includes the mechanical parts of its boards (e.g., front panel, screws, etc.) plus the sub-rack that holds them together, the whole being modeled by its total mass.

Each RU of the BS contains the analog front-end (AFE) and the power amplifiers (PAs) for one cell. The AFE performs specific analog functions in transmission, i.e., digital-to-analog conversion, up-conversion and pre-driving, in reception, i.e., low-noise amplification, down-conversion and analog-to-digital conversion, and for the whole cell, i.e., frequency synthesis, clock generation and general control. The PAs amplify the radio signals before they are emitted by the antennas (Golard et al. 2024). RUs can be classified into several categories according to two main aspects. The first aspect concerns their output power: macro RUs emits from 40 W to >100 W per cell, compared with 1-40 W per cell for micro RUs. The second aspect relates to their location: radio frequency units (RFUs) are installed within the BS cabinet next to the BBU, while remote radio units (RRUs) are installed closer to the passive AUs to reduce losses in the cables connecting them together. In general, a RU supports different communication protocols but are optimized for a specific one (e.g., a TDD-RRU at 3.5 GHz is specific to 5G-NR). The AFE and PA functions are performed by electronic sub-components which we distinguish into four parts: the power supply, the processing units, the transceivers (TRXs) and the amplifiers, for which the quantities are once again modeled by the surface area of their PCBA. The mechanical structure of the RU combines a casing with heat sinks to ensure effective heat dissipation. It also supports the cavity filters which are commonly used in RUs for their ability to handle high amounts of power with low losses (Hunter et al. 2002). This whole structure is modeled through its total mass.

The AU radiates the radio frequency signals amplified by the RU and receives the signals emitted by the mobile terminals. A single AU usually covers a unique sector and consists of several two-dimensional antenna arrays, each handling a dedicated frequency band. An antenna array contains multiple radiating antenna elements (AEs) arranged in rows and columns and split into sub-arrays. MIMO antennas with multiple sub-arrays are required to implement adaptive beamforming (ABF) (Tahseen et al. 2023). The electronic sub-components of the AU are the AEs comprising all the radiating elements plus the internal cables and the delay lines used to control the delay in radio-frequency signals. The whole is modeled by the total mass. The mechanical structure of the AU consists of a reflective plane which focuses the radiation pattern of the antenna and supports the AEs, plus a radome to protect AEs from outdoor conditions. To calculate the total mass of a traditional AU structure, we consider that antenna arrays from different frequency ranges (e.g., 0.8 and 1.8 GHz) are superimposed to save space and reduce the wind load. Yet, arrays from bands within the same frequency range (e.g., 1.8 and 2.1 GHz) cannot be superimposed because they may interfere with each other (Tahseen et al. 2023). Then, we uniformly allocate the total mass of the AU structure per supported band.

Recently, a new type of BS component has emerged in RANs: active antenna units (AAUs), combining the AFE, PAs and AEs for one cell into a single physical unit. In the BS life-cycle model, the production of this special component is split between the RU and AU production modules. The RU production module covers the production of the active electronic subcomponents, as well as the casing and heat sinks. On the other hand, the AU production module models the production of the antenna part, including the radome and AEs. Thus, the RU part of the AAU is modeled like a traditional RRU, and the modeling of the AEs does not change in the AU module. However, the mechanical subcomponents modeled by the AU module consists only of the radome with AAUs because the reflective plane corresponds to one side of the RRU casing. Moreover, we consider that a single AAU supports only one frequency band, thus eliminating the need for mass allocation between bands. Since the antenna array of an AAU cannot be superimposed on other antenna arrays, AU modules for cells using AAUs are modeled independently. Therefore, they do not affect the mass calculation of the mechanical structure of traditional passive AUs for the other cells.

The PSU supplies power to the BBU and all RUs of the BS. Since the available electrical power source is usually low-voltage alternating current (AC) and as the BS components operate on direct current (DC), the PSU handles AC/DC conversion and power distribution to all BS components (May 2006; Golard et al. 2024). Hence, the first electronic sub-component of the PSU relates to the power conversion and comprises multiple rectifiers, a power distribution panel, a controller, and fans for active cooling. The PSU may also include backup batteries to guarantee a reliable service in case of a power supply failure (May 2006). These two sub-components are modeled by their mass. The mechanical structure of the PSU consists of the complete structure and casing of the BS cabinet plus the sub-rack that houses electronic sub-components of the PSU, the whole being also modeled through its total mass. Note that the production of additional components required to power isolated BSs with a diesel generator or a photovoltaic (PV) system, e.g., additional storage batteries, converters, etc., is not included in the PSU production module, but rather in the calculation of IAFs for the use stage.

Two types of external cables are required to connect all the BS components together: data cables (i.e., optical fibers and coaxial cables) and power cables. Optical fibers are used to transfer digital data between the physical-layer boards in the BBU and the RUs of corresponding cells. Coaxial cables are then used to transfer the modulated and amplified analog signals between each TRX and the corresponding sub-array in the AU. Power cables carry the electrical power between the PSU and all other active BS components (Denker 2013). The quantity of each cable is modeled with respect to its length, and we consider that the power cables supplying the BBU are already included in the PSU module. As the cables are the end products installed on site, no further assembly nor upstream transport is considered for these components.

3.2.3 Distribution stage module

The distribution stage includes the transport of BS components from their assembly factory to the specific site where they operate, plus their installation on site. The transport is divided in two segments: (i) the international transport between the manufacturer's assembly factory and the MNO's warehouse, and (ii) the local transport between the MNO's warehouse and the BS site. The international distribution is modeled by a mix of freight transportation means for the transported mass over the international transport distance (in kg·km) like the upstream transport of sub-components. The mass of each component is calculated by summing the mass of all its sub-components. On top of this, we add the mass of the specific packaging that we no longer consider negligible for worldwide freight. The international distribution distance depends on where the BS components are manufactured and where the MNO is based. As with most of today's electronics, we assume that all BS components are manufactured and assembled in East Asia (Yeung 2022). The local distribution is handled by a small truck, the impacts of which are all allocated to the BS as we consider that the entire round-trip is dedicated to the BS installation (and no longer allocated with respect to the mass, as for international freight). The installation of BS components on site consists of manual handling, assembly of mechanical parts, cable connections and system configuration, all carried out by one or more technicians. As for the component assembly, we simply model the BS installation by electricity consumption, with a wide range of uncertainty due to a lack of primary data. We consider that the technicians travel in the same truck as the BS.

3.2.4 Use stage module

The use stage of the BS consists solely of electricity consumption since support activities, e.g., maintenance, are excluded from the scope of the model. Various electricity sources can be used to supply the BS, and our model allows to choose between three typical ones: the electricity grid, a diesel generator, or a PV panel system. The last two options are generally used by isolated off-grid BSs (Malmodin et al. 2018; Malmodin et al. 2024). The instantaneous BS power consumption varies over time depending on the traffic load, e.g., the average BS load is typically lower in the night than in the afternoon (Golard et al. 2023). Typically, the average hourly load ranges from 0 to 30% (Golard et al. 2023), but the BS load profile may evolve over the years as the overall data traffic increases. To model BS energy consumption, we reuse our parametric power model proposed in Golard et al. (2024), since the scope and modeling approach of that work are close to this LCA study, in addition to using a similar set of model variables. The total energy consumption of the BS is calculated over its whole lifetime.

3.2.5 End-of-life stage module

The end-of-life stage is difficult to model because we lack primary data and there is no clear consensus in the literature on the modeling of e-waste management (Ficher et al. 2024). We therefore propose a streamlined modeling approach for this stage. In the following, we only consider the formal waste management of BSs, assuming a 100% collection rate, as they are managed by companies subject to strict e-waste management legislation such as the directive EU 2012/19/EU (2012). The first steps of end-of-life mirror the local part of the distribution stage, i.e., the de-installation of the BS from the site and the local transport back to the MNO's warehouse (i.e., the local collection). Next, we assume that all BS components are disassembled and separated into electronic sub-components on one side, and mechanical sub-components on the other. This step is modeled as the counterpart to the assembly of BS components, using the local electricity grid mix. Waste management is assumed to take place in the same region as the BS use, meaning that no international transport is required, but downstream transport is considered and modeled as the upstream transport.

At this point, several waste management routes can be envisaged, such as in Scharnhorst et al. (2006b). We consider that the default route for all BS materials is disposal by incineration and landfill. This is a pessimistic modeling option because no process and associated environmental impacts can be "cut-off" from the product system (e.g., material recovery processes). The other more environmentally friendly route of the model is waste recycling under market capabilities. Indeed, the use of recycled materials in another product system reduces its production impacts, as shown by Scharnhorst et al. (2006b) for a BS rack. However, assessing recycling using the open-loop substitution approach leads to the invisibilization of recycling processes and a potential underestimation of end-of-life impacts (Ficher et al. 2024). It means that the recycling route, especially in open loop, is an optimistic modeling option. We hence argue that a realistic assessment of the end-of-life lies somewhere between the two options. The impacts of both waste management routes are assumed to be proportional to the mass of waste processed.

3.3 Impact assessment factors

The IAFs contained in vectors $F_k(x)$ are used to compute the environmental impacts associated with each foreground process (see Section 2.1). As shown in Figure 4, IAF calculations rely on background processes built on the unit processes from the ecoinvent database (unit processes are referred to as "dataset" in the ecoinvent documentation). In general, we use the "market for" unit processes to represent the average market composition and to include transport, except when considering specific raw material mixes for which we determine the share of virgin and recycled materials. We rely on global average (i.e., "GLO") unit processes when the value chain of a process is assumed to be global, when the process location is unknown, or when a regionalized unit process is unavailable in ecoinvent. We additionally develop custom unit processes to model the production of ICs, connectors, and PAs. The main data sources for building the background processes are teardowns, technical documentation, and bill-of-materials of various BS components. Since these sources lack completeness in relation to the model's validity domain, we assume static IAFs rather than parametric ones, meaning that $F_k(x) = F_k$, which implies additional uncertainty, as discussed in Section 3.4.

The rest of this section explains the main assumptions we made to calculate the IAFs and discusses the results shown in Figure 5 for the global warming potential (GWP). An equivalent figure for abiotic resource depletion potential (ADP) is presented in Online Resource 1. Further details on how we build background processes based on ecoinvent and custom unit processes are also provided in Online Resource 1. The complete list of unit processes used to calculate all IAFs is given in Online Resource 2.

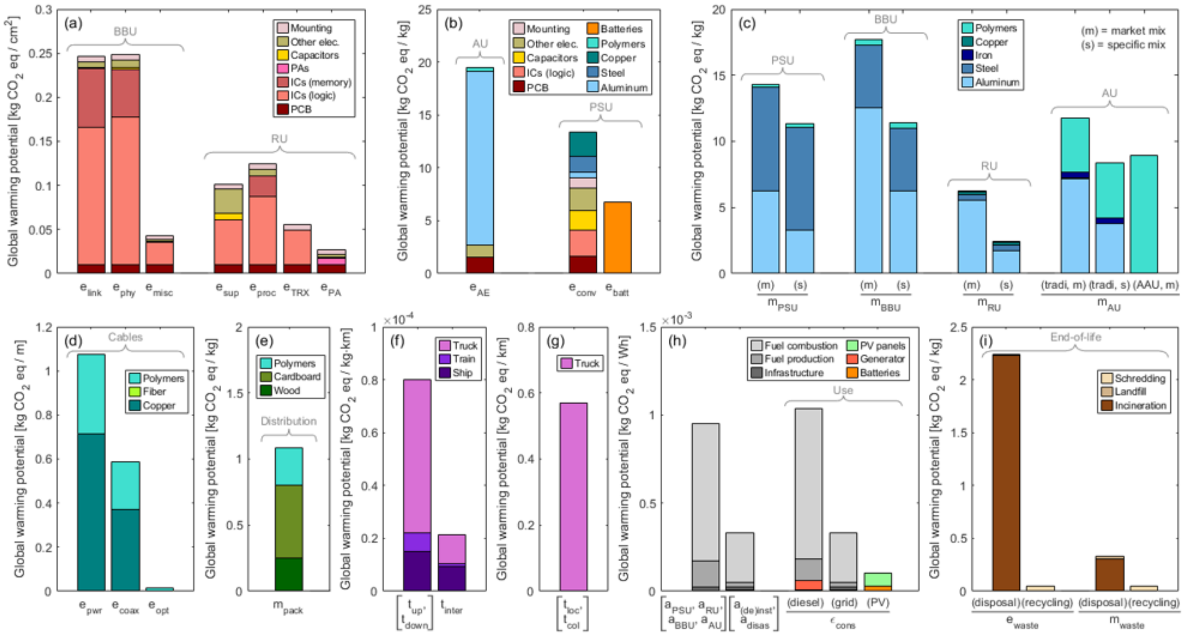

Fig. 5 Global warming potential of all foreground processes for (a) printed circuit board assembly production, (b) other electronic production, (c) mechanical structure production, (d) cable production, (e) packaging production and disposal, (f) freight transport, (g) local transport, (h) electricity consumption, and (i) waste management routes. Some impact factors apply to several processes (in brackets), while other processes may be linked to different impact factors depending on the model options (in parentheses)

3.3.1 Printed circuit board assemblies

A PCBA typically consists of a printed circuit board (PCB) on which active and passive electronic components are mounted. Most of the active components are logic and memory ICs, while the passive components are mainly inductors, capacitors, resistors, and connectors.

We use our own detailed teardowns of a BBU and a RRU to study the composition of their PCBAs. Since these compositions vary significantly depending on the function performed, we calculate specific IAFs for the different types of PCBAs considered in the FPI (see Table 2). For that, we first separate the PCBAs of the BBU (resp. RRU) into three (resp. four) parts according to the function performed by each PCBA region. Then, we list all the electronic components present on these parts and add the PCB mounting processes including the solder paste. Lastly, we allocate all these processes per cm² of PCB surface area. The mass density of PCBAs is estimated around 1 g/cm².

Figure 5(a) shows that the GWP per cm² of PCBAs varies by around an order of magnitude, from 0.03 kg CO_2 eq for providing basic analog functions and up to 0.25 kg CO_2 eq for performing complex digital functions. This difference is explained by a higher density of high-impact components such as digital ICs (for logic and memory) in the link- and physical-layer boards of the BBU. On the other hand, PCBAs performing analog functions as for TRXs and PAs have a moderate component density to reduce noise and control the impedance of the routing lines (Eastman 1996). Nevertheless, ICs implementing analog functions still have a high manufacturing impact as, e.g., in PAs due to the use of precious metals like gold and silver. The PCBAs supporting power supply and miscellaneous functions have low to moderate impacts on climate change, reflecting a high density of low-impact components (e.g., capacitors, inductors, and small ICs).

3.3.2 Other electronics

Based on our own teardown of a traditional AU, the radiating elements of the AEs are primarily made up of aluminum sheets and polymer parts. The delay lines consist of a non-populated PCB plus a few polymer parts housed in a die-cast aluminum casing. Internal coaxial cables transmit the signal from the external connectors of the AU to the AEs through the delay lines. Whatever the AU type (traditional or AAU), we assume that aluminum sheets are used for all radiating elements below 6 GHz. Moreover, we assume that only primary aluminum is used to manufacture AEs as they presumably need to be of high purity in order not to degrade radio-frequency signals, like other electronic sub-components. Figure 5(b) shows that the aluminum accounts for more than 80% of the GWP of AEs.

The two electronic sub-components of the PSU are modeled using proxies from ecoinvent scaled with respect to their mass, as we could not get a PSU for tearing it down by ourselves. For the power converter sub-component, we chose in ecoinvent the unit process modeling the production of an inverter for a PV system comprising transformers, control units, connectors, etc. Indeed, for a similar rated power magnitude (2.5 kW in this case), we assume a similar composition between an inverter and a rectifier as they perform opposite yet comparable functions (the former converting power from DC to AC, the latter from AC to DC). In Figure 5(b), the impact from copper is due to the wires and the rest to the other electronic components. For the backup battery pack, we consider an even mix of lithium-ion and lead-acid batteries as these two technologies currently coexist in PSUs for BSs. Note that lithium-ion batteries have a higher energy density than lead-acid batteries and thus a higher GWP per kilogram of battery.

3.3.3 Mechanical sub-components

The material compositions of all mechanical sub-components are determined using the teardowns of BS components and equipment documentation from BS manufacturers. During our own teardowns, the different materials were identified based on their appearance, magnetic properties, density, etc. Two types of aluminum are encountered with different manufacturing processes: aluminum sheets and aluminum die-cast parts. The other metals identified are steel, iron and copper. We assume that most of the polymer parts are made of acrylonitrile-butadiene-styrene, and that polyamide is used for glass fiber-reinforced plastic. In all cases, the use of a raw material from the technosphere is coupled with a processing step to produce the desired mechanical element, e.g., injection molding for polymers. The PSU and BBU casings are generally made of steel and aluminum sheets, while the RU casing is made of die-cast aluminum. An internal part of the RU structure is also copper plated for the realization of cavity filters. Conversely, the radome of traditional AUs is made of reinforced plastic to be transparent to radio waves and is mounted on an aluminum structure including the reflective plane. For AAUs, only the radome is considered in the AU since the rest of the structure is modeled by the RU (see Section 3.2.2).

As explained in Section 3.2.1, we consider two options for the materials sourcing of mechanical sub-components: a market mix and a specific mix containing more recycled materials. By default, market mixes (as modeled by ecoinvent) are assumed for all materials, and only aluminum benefits from the option of a specific material mix. The underlying reason is that this option is simple to implement using ecoinvent as a unit process for aluminum scrap recycling is directly available, unlike for other materials. Yet, this limitation is balanced by the fact that aluminum is the material that accounts for most of the GWPs in Figure 5(c), justifying a priority attention. Thereby, we define a closed-loop recycling scenario for aluminum, assuming an optimistic scrap utilization of 95% (Paraskevas et al. 2015). Thus, 95% of the aluminum mass in BS components is recovered after recycling to produce a new BS component. The remaining recycling plus manufacturing losses are covered by additional aluminum from the market. Figure 5(c) shows that the higher use of recycled aluminum reduces the GWP of mechanical structures by one-third to two-thirds compared to the current average mix of raw aluminum.

3.3.4 Cables

As the ecoinvent database lacks granularity and specificity for cable production, we develop specific cable models for the BSs. For the power and coaxial cables, our teardowns help to quantify the mass of main material categories, while their precise compositions are estimated thanks to bill-of-materials disclosed by manufacturers. For the optical fiber cable, a single bill-of-material is used to build the background process.

Figure 5(d) shows that the GWP per meter of cables is dominated by copper when it is used, which is the case for coaxial cables and especially power cables. Moreover, there is a difference of two orders of magnitude between the GWP of optical fiber and power cables. In fact, this partly reflects the difference in linear density between all these cables (around 160 g/m, 90 g/m and 4 g/m for respectively the power, coaxial and optical fiber cables).

3.3.5 Packaging and transport

According to equipment documentation from BS manufacturers, the average packaging mass is composed of 55% wooden pallets, 40% corrugated cardboard box and 5% polymers. Yet, cardboard and polymers account for most of the packaging's GWP, as illustrated in Figure 5(e). Upstream and downstream transports are modeled with the same distribution of freight transportation means (per kg·km): 37% truck, 15% train, 24% inland barge and 24% container ship (ITF 2022). Using the same approach, the international transport is modeled considering 91% container ship, 7% truck and 2% train (Bucsky 2019). In Figure 5(f), the GWP per kg·km of the upstream (or downstream) transport is higher than that of the international transport due to the higher share of road transport. Indeed, road transport has the highest GWP, around 0.16 kg CO_2 eq/t·km, compared to around 0.05 and 0.01 kg CO_2 eq/t·km respectively for rail and container ship. Finally, Figure 5(g) indicates the GWP per km traveled for the local distribution and collection, which is handled exclusively by small trucks entirely dedicated to transporting BS components.

3.3.6 Electricity consumption

IAFs for the electricity consumed by the final assembly of BS components are modeled by the medium-voltage electricity grid mix in China, which we assume to represent the electricity mix in East Asia. On the other hand, we consider the European low-voltage grid mix for the electricity used for the installation, de-installation and disassembly of the BS. This therefore applies to a BS deployment in Europe, but we suggest adapting this electricity mix to the specific region of deployment.

Three power supply options are proposed for the use stage energy consumption: the electricity grid (default option), a diesel generator, or a PV panel system. The electricity grid mix in Europe is considered with the same comment as before regarding the location of the BS site. The modeling of electricity grid mixes is directly taken from ecoinvent. For diesel power generation, we include the impacts of producing the generator, producing the fuel, the direct emissions from combustion, and the production of additional batteries. The PV system model includes the production of PV panels and additional batteries. The additional batteries are sized to store up to one and three complete days of BS energy consumption for the diesel and PV systems respectively. We assume the use of lithium-ion batteries only due to their high energy density and long lifetime (Lai et al. 2024). The IAFs for these three options are calculated per Wh of energy consumed, yielding GWPs of around 1000, 950, 330 and 100 g CO_2 eq/kWh for the diesel generator, Chinese grid, European grid and PV system respectively (see Figure 5(h)). As expected, direct emissions dominate the GWP when electricity is partly generated from fossil fuels. GWP is very high when coal is the principal energy source as in China, whereas in Europe more renewable and nuclear energy sources are used in addition to fossil gas (Scarlat et al. 2022). Conversely, the GWP of the PV system is mainly due to the production of PV panels, meaning that impacts per Wh are largely influenced by the power system lifetime, which we assume to be 30 years (Tao and Yu 2015), hence greater than the BS lifetime.

3.3.7 Waste management

After de-installation, local transport and disassembly, the waste management of electronic and mechanical sub-components is modeled for two different routes. The first route is the disposal by incineration and landfill, for which we estimate the average mass composition of waste from mechanical and electronic sub-components as respectively: 70% aluminum, 10% polymers, and 20% of other materials, and 35% PCBAs, 40% batteries, and 25% cables. To calculate IAFs of the incineration of these wastes plus the following landfill of residues and bottom-ash, we use the unit processes in ecoinvent that correspond (or at least are the closest) to the specific waste compositions. As ecoinvent still considers the recycling of some residues after incineration (and hence cut them off), we add their landfill to the IAF calculations. The second waste management route is recycling by first shredding the waste, of which 95% is then available for material recovery (and hence cut-off) and 5% is lost and landfilled. The recycling routes of both types of waste are modeled in the same way considering waste shredding plus the landfill of the few losses. Figure 5(i) shows that most of the GWP of disposal comes from the incineration. The GWP of e-waste incineration is also greater than for waste of mechanical sub-components because they contain more materials to burn and thus emit more GHGs compared to, e.g., metals. For both types of waste, the impacts of preparing materials for recycling (before cut-off) are mainly due to shredding, as modeled in ecoinvent (Hischier et al. 2007). Thus, the GWP of the recycling route is at least one order of magnitude lower than that of the disposal route.

3.4 Uncertainty quantification

Previous sections only provide *deterministic* parametric models and parameter point estimates that are supposed to represent "typical" or "most representative" foreground processes. In this section, our goal is to quantify the uncertainty in the proposed BS life-cycle model by introducing a *stochastic* dimension. Yet, we only address model-specific uncertainty (i.e., uncertainty related to the FPI and IAF calculations), but does not cover external uncertainty (e.g., uncertainty in the LCI of ecoinvent or the EF 3.1 method). Therefore, the uncertainty quantification does not encompass the full range of uncertainties, from quantitative temporal variability to qualitative epistemological uncertainty, as outlined by Hauschild et al. (2018).

In the BS model, the uncertainty of each foreground process quantity and IAF vector (i.e., $q(x)$ and $F(x)$) is modeled by a lognormal distribution. This distribution is chosen for three reasons: (i) it is positive definite, which is consistent for process quantities and IAFs, (ii) it allows for the analysis of multiplicative order-of-magnitude uncertainty rather than additive symmetrical uncertainty, and (iii) it fits well with the empirical residuals from regression analyses of the specific data sources. The medians of the lognormal distributions are set to the deterministic model predictions, and their geometric standard deviation (GSD) reflects the associated stochastic uncertainty. For instance, a GSD of 1.40 corresponds to a lognormal distribution with an interquartile range (IQR) ranging from -20% to $+25\%$ relative to the median.

According to Heijungs (2024), the uncertainty in LCA results stems from two main sources: the *variability* (e.g., in process quantities, between years, between manufacturers, etc.) and the *error* (e.g., in the use of proxies to calculate IAFs, in the model structure, due to a lack of primary data, etc.). In the BS model, lognormal distributions for these two parts of the uncertainty are determined separately for each foreground process quantity and IAF vector. The GSD representing the variability part is calculated by fitting a lognormal distribution to the relative residuals from the regression analysis of specific data sources (when sufficient data is available). Next, the error part is based on our own judgment of confidence in the modeling of the foreground processes and associated statistical variability. The corresponding GSD indicates the magnitude of potential error that the modeling approach may introduce in LCIA results. The GSD factor representing the total uncertainty is then calculated by combining the variability and error GSD factors, assuming independent lognormal distributions as in Limpert et al. (2001).

Table 3 provides the GSD factors for the FPI and IAF uncertainties for each (type of) foreground process. These factors are presented separately for the variability and error parts in order to distinguish statistically calculated GSDs from GSDs based on our own judgements. FPI variability factors cannot be calculated for processes that lack a primary data source (e.g., assembly), which leads to a higher error factor for these processes. Similarly, we cannot calculate variability factors for IAFs because they are mainly based on a single teardown. Therefore, the error factors for IAFs capture the expected variability of the process composition, as well as our level of confidence in the modeling choices used to build the background processes with ecoinvent. Uncertainty quantification does not apply to distribution and collection transports at the FPI level because these transports are directly input model variables. Online Resource 1 provides more details on how both variability and error factors are calculated for uncertainty quantification.

Table 3 Uncertainty factor for the foreground process inventory and impact assessment factors expressed in geometric standard deviation

(Type of) foreground process	FPI			IAFs
	variability	error*	total	error*
electronic sub-component production	1.41	1.12	1.44	1.44
mechanical sub-component production	1.41	1.12	1.44	1.80
upstream/downstream transport	-	3.16	3.16	1.80
distribution and collection transport	n.a.	n.a.	n.a.	1.17
(dis)assembly and (de-)installation	-	3.16	3.16	1.17
energy consumption (in use stage)	1.25	1.12	1.28	1.17
waste management routes	-	1.41	1.41	3.62

* based on the authors' judgments

The overall uncertainty in LCIA results is finally calculated using Monte Carlo simulations (Hauschild et al. 2018; Heijungs 2024) with 10000 random generations. These simulations simplify mathematical operations on lognormal uncertainties and ease the propagation of uncertainty between linked parametric processes in the model (e.g., the uncertain mass of a BS component influences the transport quantity, which is itself uncertain even for a known transported mass).

4 Results and interpretations

This section presents the *interpretation* phase of the LCA, based on results obtained with the proposed BS life-cycle model applied to different sets of model variables representing typical BS configurations. This serves two main purposes: (i) to demonstrate the type and range of results that the model can produce, highlighting its flexibility, and (ii) to perform a local sensitivity analysis through a scenario analysis (Hauschild et al. 2018; Heijungs 2024). We also discuss the uncertainty associated with the results and identify the key influencing variables. In this section, the results are computed for a specific FU defined as *the provision of all communication services throughout the lifetime of an entire BS deployed in Europe*. However, the quality of service provided by the typical BS configurations may vary, which suggests that studying more specific, quality-of-service-oriented FUs could also be relevant. The influence of the FU definition is further discussed in Section 4.4.

Table 4 Typical base station configurations

Variable	3-bands*			2T2R	8T8R	64T64R	micro-4T4R	micro-16T16R
N_S	3			3	3	3	3	3
N_B	3			1	1	1	1	1
τ_{back} [hours]	0.25			0.25	0.25	0.25	0.25	0.25
d_{AU} [m]	25			25	25	25	10	10
d_{inter} [km]	20000			20000	20000	20000	20000	20000
d_{loc} [km]	500			500	500	500	500	500
$\bar{l}_{avg}$	0.1			0.1	0.1	0.1	0.1	0.1
L [years]	10			10	10	10	5	5
electricity source	diesel gen. (or PV)			grid	grid	grid	grid	grid
waste management	disposal (or recycling)			disposal	disposal	disposal	disposal	disposal
f [GHz]	0.8	1.8	2.6	1.8	3.5	3.5	1.8	3.5
B [MHz]	10	20	20	20	100	100	20	100
N_L	2	2	4	2	8	8	4	8
P_{TX} [W]	40	40	20	40	25	3.125	5	1.25
$G_{TX,dB}$ [dBi]	16	16	16	16	20	23	7	14
N_{TX}	2	2	4	2	8	64	4	16
N_{RX}	2	2	4	2	8	64	4	16
δ_{cab}	0.8	0.8	0.8	0.8	0.8	1	0.8	1
duplex scheme	FDD	FDD	FDD	FDD	TDD	TDD	FDD	TDD
protocol	4G-LTE	4G-LTE	4G-LTE	4G-LTE	5G-NR	5G-NR	4G-LTE	5G-NR
ABF	w/o	w/o	w/o	w/o	with	with	w/o	with
AU type	tradi.	tradi.	tradi.	tradi.	tradi.	AAU	tradi.	AAU
capacity [Mbps]	80+160+320 = 560			160	3200	3200	320	3200
coverage [km²]	min(52.6, 7.7, 2.6) = 2.6			7.7	1.1	1.7	0.4	0.1

* illustrative base case for the result interpretation (in parentheses = options for an alternative configuration)

4.1 Typical base station configurations

In Table 4, we define six examples of typical BS configurations to illustrate the rest of this section. The first four configurations correspond to macro BSs and the last two are micro BSs. They all have three sectors. The first configuration is the only one to support more than one frequency band. This serves as illustrative base case, as this configuration is very common in mobile networks. All other single-band configurations enable finer comparisons when adjusting for variables other than the number of bands. These configurations can be combined to obtain more sophisticated BS configurations. Half of the configurations operate with the 4G-LTE protocol, and the other half with 5G-NR. The latter use the 3.5 GHz band in TDD with a bandwidth of 100 MHz, and their AUs always feature ABF. AAUs are used when the number of TRXs is greater than 8. An alternative version of the 3-bands configuration is used to analyze recycling, and the switch from a diesel generator to a PV system for power supply. In all other cases, no recycling is considered, and electricity is supplied from the grid, assumed to be the average mix in Europe. We assume an average physical load of 10%, which is shown to be realistic in Malmodin (2020) and Golard et al. (2024). However, we consider that no power-saving features (e.g., sleep modes) are implemented. Thus, most of the energy consumption comes from the static power consumption of the BS (Golard et al. 2024). The lifetime of macro BSs is set at 10 years (Humar et al. 2011; Malmodin et al. 2014; Bergmark 2015; Madon 2021; Kallio et al. 2021), and we assume a lower lifetime of 5 years for micro BSs.

The two last rows of Table 4 provide the data throughput capacity and the coverage area of each BS configuration. These are calculated by considering a realistic spectral efficiency of 4 bps/Hz and by applying the modified "COST231-Hata" radio channel propagation model given by Khan (2009) in an urban environment. Details of related calculations are given in Online Resource 1.

4.2 Assessment of the production stage

As the model primarily focuses on the production stage, Figure 6(a) shows the impacts of this stage alone in the illustrative 3-bands configuration. A quick hotspot analysis reveals that the RUs dominate most impact categories, often followed by the AUs. This reflects the high number of these components, which is directly related to the number of BS cells. Power cables impact strongly certain categories due to the substantial amount of copper they contain. Impacts of electronic sub-components are mainly due to PCBA manufacturing (especially the ICs), and those of mechanical sub-components to aluminum production. Upstream transport and final component assembly are clearly negligible in all impact categories.

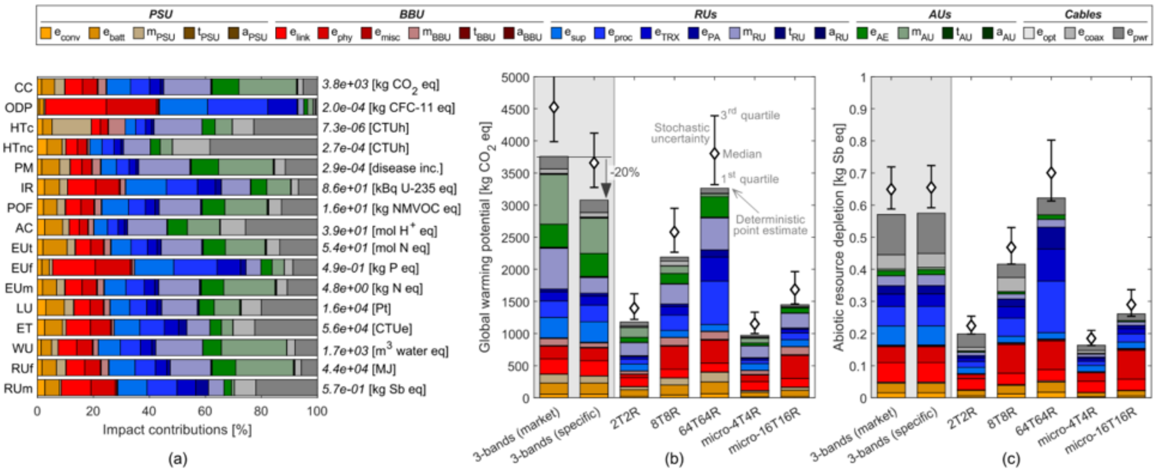

Fig. 6 Results of the production stage (a) in the 3-bands configuration for all Environmental Footprint categories: climate change (CC), ozone depletion (ODP), human toxicity – cancer (HTc) and – non-cancer (HTnc), particulate matter (PM), ionizing radiation (IR), photochemical ozone formation (POF), acidification (AC), eutrophication – terrestrial (EUt), – freshwater (EUf) and – marine (EUm), land use (LU), ecotoxicity freshwater (ET), water use (WU), and resource use – fossils (RUf) and – minerals and metals (RUm), and in all typical base station configurations (b) for the global warming potential, and (c) for the abiotic resource depletion potential

Figure 6(b) focuses on the climate change impact category and extends the results to all typical BS configurations, showing how the proposed parametric model can be used to compare different BS configurations. In single-band scenarios, the deterministic GWP of macro BS production lies between 1000 and 3500 kg CO_2 eq, which is generally higher than for micro BSs, in the range of 1000-1500 kg CO_2 eq. This difference is driven by higher output power in macro BSs, requiring larger RUs and PSUs, as well as higher antenna gains, implying more AEs and hence larger AUs. Moreover, multiplying the number of TRXs (e.g., from 8T8R to 64T64R) increases the required PCBA area in RUs and the number of AEs in AUs. In contrast, using AAUs instead of traditional AUs reduces the impact of the mechanical part of AUs. The bandwidth and the number of layers, which reflect the BS capacity, rather influence the GWP of BBU production. Furthermore, the use of recycled aluminum in the 3-bands scenario (in a closed loop with a recycling rate of 95%) reduces the GWP of its production by 20% compared to the use of aluminum from the market. Finally, among all GHGs, carbon dioxide accounts for around 85% of the GWP (see Online Resource 1), the remainder being due to methane emissions from fossil fuels as well as fluorinated gases needed for electronics manufacturing (Hess 2024).

Figure 6(c) shows the ADP results, i.e., the indicator of the "resource use – minerals and metals" category, as an example of another impact category revealing quite different trends. Overall, variations between BS configurations are like those observed for GWP, except that no savings are obtained from the use of more recycled aluminum because of other critical resources used in the metallurgical recycling processes. The major difference lies rather in the contributions of foreground processes. Compared to the GWP, the contribution of mechanical structure production is lower for ADP, reducing the AU contribution to a small fraction, while that of PCBA and power cable production increases, particularly due to the use of copper and gold. Overall, various trade-offs regarding BS designs emerge when considering the complete set of model variables and all impact categories. Therefore, we suggest using our model for further BS design optimization in future works.

In addition to deterministic results, uncertainty ranges are also displayed in Figure 6(b) and Figure 6(c) through the IQRs and medians of the stochastic assessments. According to a common rule of thumb from Heijungs (2024), a difference in results between two BS configurations can be considered significant if their IQRs do not overlap. Under this criterion, the difference in production impacts between 64T64R and micro-16T16R configurations appears significant, while no significant difference is observed between 2T2R and micro-4T4R BSs. Most of the uncertainty in the results is due to uncertainties in the FPI and IAFs for the production of electronic and mechanical sub-components. On the other hand, the high uncertainty in upstream transport and final assembly (see Table 3) is not strongly reflected in the overall uncertainty due to their very small relative contribution. Interestingly, the medians of stochastic assessments are roughly 20% higher than the deterministic point estimates, with the latter sometimes falling below the first quartile of stochastic assessments. In fact, this is due to the positive skewness of lognormal distributions that are summed to calculate the total impacts. This underlines that neglecting uncertainties in the life-cycle model could systematically lead to underestimation of potential environmental impacts.

4.3 Comparison between life-cycle stages

Including LCA modules for distribution, use, and end-of-life allows for direct comparison across all life-cycle stages. Figure 7(a) shows the GWP results per life-cycle stage in all typical BS configurations and Figure 7(b) focuses on ADP. Note that the y-axis is in logarithmic scale.

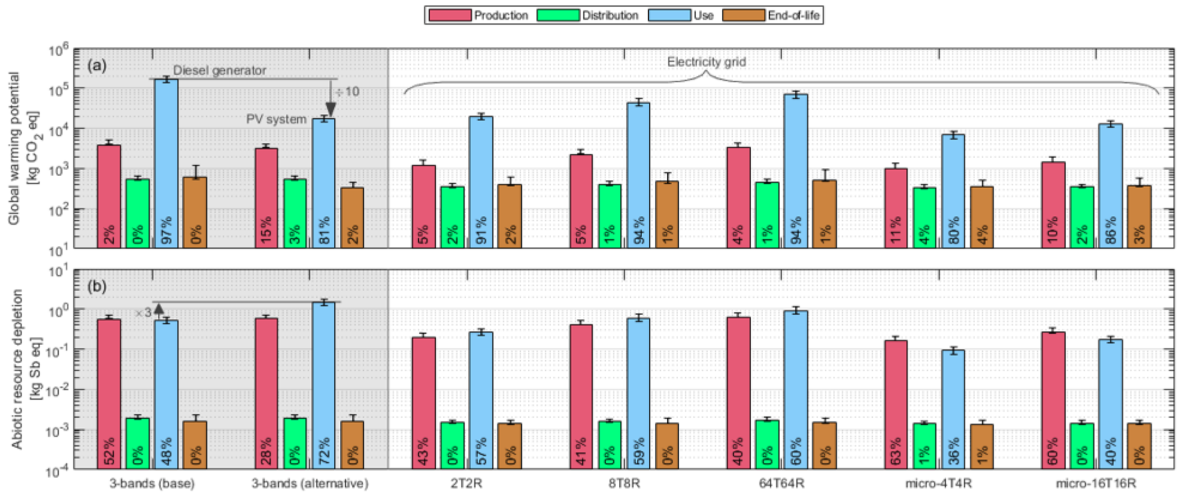

Fig. 7 Results by life-cycle stage in all typical base station configurations (a) for the global warming potential, and (b) for the abiotic resource depletion potential. For the sake of clarity, only the interquartile range of the uncertainty is displayed and not the median

Regarding climate change, the use stage is clearly the hotspot. For macro BSs, it accounts for more than 90% of the total GWP, except when powered by a PV system for which the carbon intensity is ×3 and ×10 lower than the electricity grid and the diesel generator, respectively. In any case, the GWP of the production stage never exceeds 15% of the total carbon footprint, even in the case of micro BSs. This shows that decarbonizing the electricity supply is the main lever for reducing the total carbon footprint of a BS. However, power-saving features are neglected in these results, and we therefore expect their implementation to increase the share of the production stage in total BS GWP, making this stage non-negligible in RAN deployment strategies. Recycling also reduces the GWP of production and end-of-life stages to a lesser extent. Regarding ADP, the production stage is another hotspot, accounting for up to 60% of the total impact of micro BSs. Contrary to GWP, powering BSs with a PV system is ×3 more mineral and metal resource intensive than with a diesel generator, and ×2 more than with the electricity grid (which is dominated by the copper in distribution networks). For all typical configurations, distribution and end-of-life stages are largely dominated by local transport (see Online Resource 1) and do not contribute much to the total environmental impacts of BSs.

4.4 Influence of the functional unit definition

As explained in Section 3.1, the definition of the FU can be adapted to the purpose of using our model, which may affect the obtained results and related findings. As an example, in Figure 8 we compare the GWP of the full life cycle of all typical BS configurations for two different FUs: in Figure 8(a) we use the same specific FU as defined hereabove, and in Figure 8(b) we use a more specific FU defined as *the provision of 1 Mbps of data throughput capacity over 1 km² of coverage area during 1 year by a BS deployed in Europe*. In the latter case, the total impact of the BS is uniformly allocated per FU. Moreover, the two most impacting and less impacting configurations (namely the *worst* and *best* configurations) are highlighted in Figure 8 for each FU.

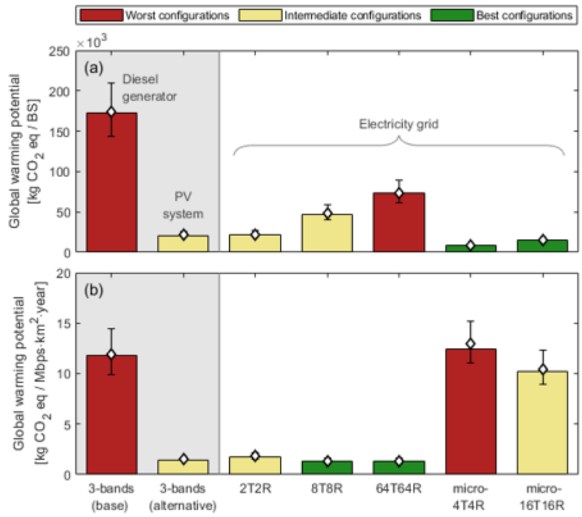

Fig. 8 Global warming potential of the full life cycle of all typical base station configurations for two different functional units: (a) all communication services throughout the lifetime of an entire base station, and (b) a specific unit of communication service from a base station

By comparing the results obtained, clear differences in trends appear between the two FUs. For example, the 64T64R BS is one of the worst configurations with the first FU and concurrently one of the best with the second FU thanks to its very high capacity. The opposite occurs with the micro-4T4R configuration due to its small coverage, short lifetime and low capacity. The emerging findings would be that deploying more and more small-scale BSs is not the best choice according to the second FU, even if their absolute GWPs per BS are the lowest with the first FU. On the contrary, the use of low-carbon electricity seems to be a good option for both FUs. Yet, other trends may emerge for other impact categories. Therefore, when comparing different BS configurations, the definition of the FU strongly influences the results and findings. It is thus of crucial importance to define a FU that suits the goal of the LCA with regard to the key services provided by the studied BSs.

5 Discussion

Comparing our results with previously published LCAs, we reach the same general conclusion that the use stage dominates the impact on climate change. However, our deterministic GWP estimates for the production of an entire BS, ranging from 1000 to 3500 kg CO_2 eq, are at the lower end of the range reported in previous studies, from 3000 to over 30000 kg CO_2 eq per BS. This can first be attributed to the exclusion of support goods and site facility construction from the scope of our model. Secondly, the use of specific data sources allows for a more detailed FPI and the calculation of specific and more realistic IAFs. Besides, no previous study enables direct comparison of our results across all other impact categories. The remainder of this section discusses the limitations of the proposed parametric model and formulates practical recommendations for its use.

5.1 Limitations

A major limitation of the model lies in the amount of specific and primary data sources, which affects its technological, geographical and temporal representativeness. This also prevents the model from capturing variability in the foreground and background systems over time, across manufacturers, and between technologies. Less information is also available for recent BS designs such as AAUs and micro BSs. These issues justify limiting the LCA scope to macro and micro sub-6 GHz BSs. In addition, certain assumptions in the FPI should be validated, e.g., the energy consumption of final assembly and installation even if their impacts appear negligible. In the background system, the use of a small number of teardowns for IAF calculations impedes a comprehensive view of the sub-component compositions. This led us to consider only static IAFs, even though they would actually vary, e.g., depending on the production year. Moreover, IAF calculations rely on ecoinvent which generally lacks geographical and technological specificity necessary for a perfect match with background processes. This results in the prevalent use of global average unit processes and the development of custom unit processes for specific electronic subcomponents (see Online Resource 1). Therefore, it may be worthwhile for future works to refine background process modeling based, e.g., on an electronics-specific LCI database.

Other limitations relate to methodological choices and to the structure of the model. First, to account for the heterogeneity of BS components, we propose a modular approach in which certain modules are defined for individual cells. This modeling choice implies that the BS is perfectly sized with respect to the model variables and especially the number of cells. In practice, however, BSs may be oversized to allow for later network upgrades. Second, the use of the cut-off perspective does not provide any benefit for recycling, which strongly favors the use of secondary materials but does not incentivize waste producers to maximize waste recycling (Wernet et al. 2016). The associated “100:0 approach” for recycling burden allocation clearly favors the first user of a material, to the detriment of the second user of the recycled material. This weighting could be adapted to be within a range of 80:20 to 20:80 to comply with EU 2021/2279 (2021), but this would require the use of another LCA database than ecoinvent. Third, we could have considered other specific raw material mixes in addition to aluminum such as for electronics and polymer production. However, this would require a more detailed analysis of waste management routes, as well as the provision of the associated specific processes in the databases. For the same reason, end-of-life modeling remains highly streamlined.

To partly address these limitations, we quantify the uncertainty associated with the model and numerical estimates in Section 3.4, which in turn enables uncertainty and sensitivity analyses. We believe this step is essential to evaluate and communicate on the accuracy of LCA results and conclusions. Users of the model are also encouraged to perform a more comprehensive sensitivity analysis tailored to their specific use case, focusing on the most influential model variables.

5.2 Practical recommendations

The proposed BS model can be used as a building block to study larger product systems such as *ICT networks* and *ICT services*, defined by ITU-T L. 1410 (2014) as logical structures physically made up of *ICT goods* and relying on building premises, civil works to create cable ways, air conditioning, etc. These additional products must therefore be modeled alongside the BS. Similarly, if the BS model is used to study the upgrade of an existing RAN, it may not be necessary to include all the LCA modules within the scope of the study. For instance, the addition of a frequency band on an existing site could be limited to the deployment of RU and AU components with a reuse of existing cables, BBU and PSU.

This reasoning then leads to questions like "how to allocate the impacts of shared infrastructure between several BS?" or "should we also attribute to a new BS a share of impacts from the previous construction of the pylon and other site facilities?". In fact, this raises the question of whether the *consequential* modeling perspective is more appropriate in some cases than the *attributional* one. In this context, we note that “while the background system is modeled differently in attributional and consequential LCA, the foreground system is overall modeled in the same way” (Hauschild et al. 2018). This means that, thanks to the flexibility of our BS model, it would be correct for a consequential LCA to keep the same FPI as proposed and simply recalculate the IAFs on the basis of marginal (and no longer average) environmental impacts. We leave it up to the model's users to decide how to deal with these issues but draw attention to the need to treat them carefully.

Regarding small-scale BSs, a greater integration of BS components into compact designs can be assumed, as well as a transformation of manufacturing processes for mass production. In that case, the reference parameter values and the scaling exponents should both be adjusted in the parametric modeling approach. Additionally, merging the production modules may be appropriate, considering that small-scale BSs are designed to fit into a single compact casing. Furthermore, to account for RAN virtualization, cloud RAN and open RAN (Lehr et al. 2021), the proposed BS model could be adapted, primarily with regard to BBU modeling. This would involve separating the BBU into a distributed unit installed at the BS site, close to the RUs, and a centralized unit installed in a data center shared by several BSs.

If the BS model is intended to inform decisions about the design and deployment of next-generation BSs, emerging technologies must also be considered. In this case, the principles of *prospective* LCA proposed by Arvidsson et al. (2018) should be applied, i.e., prospective modeling of both foreground and background systems, as well as the inclusion of technology alternatives beyond the current state of the art. The stage of technological development to consider depends on how far into the future the prospective study is carried out. Again, the inherent distinction between FPI and IAFs enables the BS model to be adapted to such a prospective LCA. For instance, we could adjust the numerical parameters of the FPI to account for expected technical improvements, e.g., reducing the PCBA surface area in the reference situation. At the same time, the technosphere may evolve in a way that alters the background model, which would require recalculating the IAFs, e.g., for the electricity grid, IC manufacturing, or market mixes of primary versus recycled raw materials.

Another well-known limitation of LCA studies is data availability (Hauschild et al. 2020; Ghose 2024). In developing the BS life-cycle model, we rely partly on confidential data sources that cannot be disclosed. Nevertheless, collecting data for any ICT-related process is time-consuming and would benefit from publicly available open-source FPIs data from network equipment manufacturers, network operators and Internet service providers. Therefore, we recommend that future works strive to open up access to as much FPI data as possible. To this end, Ghose (2024) examines data-sharing principles in terms of findability, accessibility, interoperability, and reusability.

Finally, we remind that LCA serves to evaluate the *eco-efficiency* of the product system according to an established FU (Hauschild et al. 2020). While this relative perspective helps to reduce the environmental impacts of the BS, it does not assess whether these impacts are sustainable or not with respect to the planetary boundaries (Richardson et al. 2023). Within this context, the *absolute sustainability* approach must be adopted by considering allocation principles to share the safe operating space (Hjalsted et al. 2021) in order to identify which portion of this space can be allocated to, e.g., the RAN.

6 Conclusion

This paper presents a parametric life-cycle model for assessing the environmental impacts of up-to-date commercial BSs providing wireless communication services. The proposed model aims to enable researchers, MNOs and network equipment manufacturers to compare the environmental impacts of different BS configurations, eco-design next-generation BSs, and support decisions on more sustainable RAN deployment strategies. Although the model covers the full life cycle, from raw material acquisition to end-of-life, it primarily focuses on the production stage, an aspect often overlooked in previous studies. The modular and parametric modeling strategies allow for configurability through multiple variables representing features controlled by MNOs and operating conditions imposed by the users. The model is structured into a foreground system, in which the foreground process quantities are modeled using parametric functions, and a background system, in which the impact factors are calculated using ecoinvent 3.10 with the multi-criteria LCIA method EF 3.1. Realistic numerical values for model parameters are estimated from regression analyses based on specific data sources, enabling quantitative comparisons between BS configurations.

When applied to six typical configurations of 4G and 5G cellular BS, the model shows that the use-stage energy consumption dominates the climate change impact category, regardless of the electricity source. This stage accounts for 80% to over 95% of the total GWP over the full life cycle, consistent with previous studies. The production stage contributes 1000 to 4000 kg CO_2 eq to the GWP per BS, primarily due to the production of electronic sub-components. These results are at the lower end of the range reported in previous studies. Conversely, for ADP, the production stage may dominate the use stage, contributing 30% to 60% of the total impact. For all impact categories, the distribution and end-of-life stages are negligible. These results highlight the importance of a multi-indicator analysis to avoid burden-shifting between life-cycle stages or BS components. Uncertainty in the model is quantified by combining variability in regression-based modeling with modeling error, which is assessed based on the authors' judgments. For the production stage, Monte Carlo simulations yield results with an IQR of approximately ±20% around the median. Stochastic impact assessment results exceed deterministic results by approximately 20% due to the positive skewness of lognormal distributions used to model uncertainty.

The most effective strategy for mitigating the BS impact on climate change impact is to reduce the carbon intensity of the electricity they consume during the use stage. Material choices in BS manufacturing, particularly those involving copper and gold, are also critical to reducing the use of mineral and metal resources. In contrast, increasing the share of recycled aluminum in production or recycling BSs at the end-of-life has a relatively small effect on total environmental impacts. The definition of the FU also influences comparative results: while micro BSs show lower absolute impacts, macro BSs provide greater coverage and data throughput capacity, thereby reducing their relative impacts per unit of communication service. Overall, trade-offs emerge at the RAN level between increasing capacity per BS, densifying the network, and reducing absolute environmental impacts.

From a broader perspective, this work illustrates the relevance of modular and parametric LCA models for analyzing complex, evolving, and heterogeneous product systems under uncertainty. Additionally, it shows that clearly distinguishing between foreground and background systems enhances modeling transparency and facilitates future refinements. Thanks to their flexibility and reusability across a wide range of applications, such models lay the foundations for prospective studies aimed at informing technological transitions, industry strategies, and regulatory policies.

Declarations

Data availability Processed presentations of the data supporting the results of this study are available in the Supplementary Information. Part of the raw data is used under license for this study and is subject to availability restrictions. Access to the licensed ecoinvent version 3.10 database is required to calculate the results of this study.

Author contributions (following the CRediT taxonomy) Louis Golard, Robin Dethienne: conceptualization, methodology, investigation, resources, software, writing. Jérôme Louveaux, David Bol: conceptualization, methodology, resources, writing, supervision.

Funding This study was supported by Proximus, by the EECONE project funded by the Chips Joint Undertaking under grant agreement 101112065, and by the Fonds européen de développement régional (FEDER) and the Wallonia within the Wallonie-2020.EU Program.

Competing interests The authors have no relevant financial or non-financial interests to disclose.

References

Andreasi Bassi S, Biganzoli F, Ferrara N, Amadei A, Valente A, Sala S. and Ardente, F (2023) Updated characterisation and normalisation factors for the Environmental Footprint 3.1 method. Publications Office of the European Union. https://doi.org/10.2760/798894

Arvidsson R, Tillman AM, Sandén BA, Janssen M, Nordelöf A, Kushnir D, Molander S (2018) Environmental assessment of emerging technologies: Recommendations for prospective LCA. J Ind Ecol 22(6):1286-1294. https://doi.org/10.1111/jiec.12690

Aubet L, Rabot A, Bitard L, Riolo C (2024) Empreinte environnementale de la fourniture d'accès internet en France. ADEME. https://librairie.ademe.fr/industrie-et-production-durable/6789-evaluation-de-l-empreinte-environnementale-de-la-fourniture-d-acces-a-internet-en-france.html. Accessed 15 October 2024

Bergmark P (2015) Life cycle assessment of an LTE base station based on primary data. Third ETSI Workshop on ICT Energy Efficiency and Environmental Sustainability. https://docbox.etsi.org/workshop/2015/201506_EEWORKSHOP/SESSION03_LCA/LCA_of_LTE__based_station_primary_data_Bergmark_Ericsson.pdf. Accessed 15 October 2024

Bieser J, Salieri B, Hischier R, Hilty L (2020) Next generation mobile networks: Problem or opportunity for climate protection? University of Zurich, Empa. https://doi.org/10.5167/uzh-191299

Björnson E, Sanguinetti L, Hoydis J, Debbah M (2015) Optimal design of energy-efficient multi-user MIMO systems: Is massive MIMO the answer? IEEE T Wirel Commun 14(6):3059-3075. https://doi.org/10.1109/TWC.2015.2400437

Bordage F, de Montenay L, Benqassem S, Delmas-Orgelet J, Domon F, Prunel D et al. (2021) Digital technologies in Europe: An environmental life cycle approach. GreenIT.fr. https://extranet.greens-efa-service.eu/public/media/file/1/7388. Accessed 15 October 2024

Bucsky P (2019) The iron Silk Road: How important is it? Area Dev Policy 5(2):146–166. https://doi.org/10.1080/23792949.2019.1672571

Debaillie B, Desset C, Louagie F (2015) A flexible and future-proof power model for cellular base stations. IEEE 81st Vehicular Technology Conference (VTC Spring). https://doi.org/10.1109/VTCSpring.2015.7145603

Denker M (2013) Remote radio head systems – Requirements and concept of lightning and overvoltage protection. 35th International Telecommunications Energy Conference, Smart Power and Efficiency (INTELEC). https://ieeexplore.ieee.org/document/6663274

Desset C, Debaillie B, Louagie F (2014) Modeling the hardware power consumption of large scale antenna systems. IEEE Online Conference on Green Communications (OnlineGreenComm). https://doi.org/10.1109/OnlineGreenCom.2014.7114430

Desset C, Wambacq P, Zhang Y, Ingels M, Bourdoux A (2020) A flexible power model for mm-wave and THz high-throughput communication systems. IEEE 31st Annual International Symposium on Personal, Indoor and Mobile Radio Communications (PIMRC). https://doi.org/10.1109/PIMRC48278.2020.9217264

Ding Y, Duan H, Xie M, Mao R, Wang J, Zhang W (2022) Carbon emissions and mitigation potentials of 5G base station in China. Resour Conserv Recycl 182:106339. https://doi.org/10.1016/j.resconrec.2022.106339

Eastman NL (1996) Considerations for mixed analog/digital PCB design. Wescon. https://doi.org/10.1109/WESCON.1996.554004

Ericsson (2024) Ericsson Mobility Report June 2024. Ericsson Report. https://www.ericsson.com/49ed78/assets/local/reports-papers/mobility-report/documents/2024/ericsson-mobility-report-june-2024.pdf. Accessed 15 October 2024

ETSI ES 202 706-1 (2022) Environmental Engineering (EE); Metrics and measurement method for energy efficiency of wireless access network equipment; Part 1: Power consumption – static measurement method. ETSI Standard. https://www.etsi.org/deliver/etsi_es/202700_202799/20270601/01.07.01_60/es_20270601v010701p.pdf. Accessed 15 October 2024

EU 2012/19/EU (2012) Directive of the European Parliament and of the Council of 4 July 2012 on waste electrical and electronic equipment (WEEE). EUR-Lex. http://data.europa.eu/eli/dir/2012/19/oj. Accessed 15 October 2024

EU 2021/2279 (2021) Commission recommendation of 15 December 2021 on the use of the Environmental Footprint methods to measure and communicate the life cycle environmental performance of products and organisations. EUR-Lex. http://data.europa.eu/eli/reco/2021/2279/oj. Accessed 15 October 2024

Faist Emmenegger M, Frischknecht R, Stutz M, Guggisberg M, Witschi R, Otto T (2006) Life cycle assessment of the mobile communication system UMTS: Towards eco-efficient systems. Int J Life Cycle Ass 11:265-276. https://doi.org/10.1065/lca2004.12.193

Ficher M, Bauer T, Ligozat AL (2024) A comprehensive review of the end-of-life modeling in LCAs of digital equipment. Int J Life Cycle Ass. https://doi.org/10.1007/s11367-024-02367-x

Ghose A (2024) Can LCA be FAIR? Assessing the status quo and opportunities for FAIR data sharing. Int J Life Cycle Ass 29:733-744. https://doi.org/10.1007/s11367-024-02280-3

Golard L, Louveaux J, Bol D (2023) Evaluation and projection of 4G and 5G RAN energy footprints: The case of Belgium for 2020-2025. Ann Telecommun 78(5):313-327. https://doi.org/10.1007/s12243-022-00932-9

Golard L, Agram Y, Rottenberg F, Quitin F, Bol D, Louveaux J (2024) A parametric power model of multi-band sub-6 GHz cellular base stations using on-site measurements. IEEE 35th Annual International Symposium on Personal, Indoor and Mobile Radio Communications (PIMRC). https://doi.org/10.1109/pimrc59610.2024.10817448

Guérid J, Doré J B, Reverdy J, Reig B, Clemente A, Di Cioccio L (2022) Toward eco-design of a 5G mmWave transmitarray antenna based on life cycle assessment. Joint European Conference on Networks and Communications & 6G Summit (EuCNC/6G Summit). https://doi.org/10.1109/EuCNC/6GSummit54941.2022.9815659

Hauschild MZ, Rosenbaum RK, Olsen SI (2018) Life cycle assessment: Theory and practice. Springer, Switzerland. https://doi.org/10.1007/978-3-319-56475-3

Hauschild MZ, Kara S, Røpke I (2020) Absolute sustainability: Challenges to life cycle engineering. CIRP Ann-Manuf Techn 69(2):533-553. https://doi.org/10.1016/j.cirp.2020.05.004

Heijungs R (2024) Probability, statistics and life cycle assessment: Guidance for dealing with uncertainty and sensitivity. Springer, Switzerland. https://doi.org/10.1007/978-3-031-49317-1

Hess JC (2024) Chip production's ecological footprint: Mapping climate and environmental impact. Interface. https://www.interface-eu.org/publications/chip-productions-ecological-footprint. Accessed 15 October 2024

Hischier R, Classen M, Lehmann M, Scharnhorst W (2007) Life cycle inventories of electric and electronic equipment: Production, use and disposal. Ecoinvent documentation

Hjalsted AW, Laurent A, Andersen MM, Olsen KH, Ryberg M, Hauschild MZ (2021) Sharing the safe operating space: Exploring ethical allocation principles to operationalize the planetary boundaries and assess absolute sustainability at individual and industrial sector levels. J Ind Ecol 25(1):6-19. https://doi.org/10.1111/jiec.13050

Humar I, Ge X, Xiang L, Jo M, Chen M, Zhang J (2011) Rethinking energy efficiency models of cellular networks with embodied energy. IEEE Network 25(2):40-49. https://doi.org/10.1109/MNET.2011.5730527

Hunter IC, Billonet L, Jarry B, Guillon P (2002) Microwave filters-applications and technology. IEEE T Microw Theory 50(3):794-805. https://doi.org/10.1109/22.989963

ISO 14040 (2006) Environmental management – Life cycle assessment – Principles and framework. ISO Standard. https://www.iso.org/standard/37456.html. Accesses 15 October 2024

ITF (2022) Mode choice in freight transport. OECD Research Reports. https://doi.org/10.1787/3e69ebc4-en

ITU-T L.1410 (2014) Methodology for the assessment of the environmental impact of information and communication technology goods, networks and services. ITU Recommendation. https://www.itu.int/rec/T-REC-L.1410-201412-I. Accessed 15 October 2024

ITU-T L.1470 (2020) Greenhouse gas emissions trajectories for the information and communication technology sector compatible with the UNFCCC Paris Agreement. ITU Recommendation. https://www.itu.int/rec/T-REC-L.1470-202001-I. Accessed 15 October 2024

Jung BH, Leem H, Sung DK (2014) Modeling of power consumption for macro-, micro-, and RRH-based base station architectures. IEEE 79th Vehicular Technology Conference (VTC Spring). https://doi.org/10.1109/VTCSpring.2014.7022990

Kallio S, Okrasinski T, Salemink A, Tanskanen P (2021) From Abacus and Sundial to 5G. 12th International Symposium on Environmentally Concise Design and Inverse Manufacturing (EcoDesign)

Khan F (2009) LTE for 4G mobile broadband – Air interface technologies and performance. Cambridge University Press, United Kingdom. https://doi.org/10.1017/CBO9780511810336

Kiemel S, Rietdorf C, Schutzbach M, Miehe R (2022) How to simplify life cycle assessment for industrial applications – A comprehensive review. Sustainability 14(23):15704. https://doi.org/10.3390/su142315704

Krishnan N, Williams ED, Boyd SB (2008) Case studies in energy use to realize ultra-high purities in semiconductor manufacturing. IEEE International Symposium on Electronics and the Environment. https://doi.org/10.1109/ISEE.2008.4562913

Lai X, Wang Y, Chen Q, Gu H, Zheng Y (2024) Carbon emission assessment of lithium iron phosphate batteries throughout lifecycle under communication base station in China. Sci Total Environ 949:175123. https://doi.org/10.1016/j.scitotenv.2024.175123

Larmo A, Lindström M, Meyer M, Pelletier G, Torsner J, Wiemann H (2009) The LTE link-layer design. IEEE Commun Mag 47(4):52-59. https://doi.org/10.1109/MCOM.2009.4907407

Lehr W, Queder F, Haucap J (2021) 5G: A new future for mobile network operators, or not? Telecommun Policy 45(3):102086. https://doi.org/10.1016/j.telpol.2020.102086

Limpert E, Stahel W A, Abbt M (2001) Log-normal distributions across the sciences: Keys and clues: on the charms of statistics, and how mechanical models resembling gambling machines offer a link to a handy way to characterize log-normal distributions, which can provide deeper insight into variability and probability – Normal or log-normal: That is the question. Bioscience 51(5):341-352. https://doi.org/10.1641/0006-3568(2001)051[0341:LNDATS]2.0.CO;2

Lorincz J, Matijevic T (2014) Energy-efficiency analyses of heterogeneous macro and micro base station sites. Comput Electr Eng 40(2):330-349. https://doi.org/10.1016/j.compeleceng.2013.10.013

Lundén D, Malmodin J, Bergmark P, Lövehagen N (2022) Electricity consumption and operational carbon emissions of European telecom network operators. Sustainability 14(5):2637. https://doi.org/10.3390/su14052637

Madon M (2021) Developing a parameterized embodied emissions calculator for telecommunication networks equipment (PEEC). Dissertation, KTH School of Electrical Engineering and Computer Science

Malmodin J, Lundén D, Moberg Å, Andersson G, Nilsson M (2014) Life cycle assessment of ICT: Carbon footprint and operational electricity use from the operator, national, and subscriber perspective in Sweden. J Ind Ecol 18(6):829-845. https://doi.org/10.1111/jiec.12145

Malmodin J, Lundén D (2018) The energy and carbon footprint of the global ICT and E&M sectors 2010-2015. Sustainability 10(9):3027. https://doi.org/10.3390/su10093027

Malmodin J (2020) The power consumption of mobile and fixed network data services: The case of streaming video and downloading large files. Electronics Goes Green 2020+ (EGG). https://online.electronicsgoesgreen.org/wp-content/uploads/2020/10/Proceedings_EGG2020_v2.pdf Accessed 15 September 2025

Malmodin J, Lövehagen N, Bergmark P, Lundén D (2024) ICT sector electricity consumption and greenhouse gas emissions-2020 outcome. Telecommun Policy 48(3):102701 https://doi.org/10.1016/j.telpol.2023.102701

May GJ (2006) Standby battery requirements for telecommunications power. J Power Sources 158(2):1117-1123. https://doi.org/10.1016/j.jpowsour.2006.02.083

Paraskevas D, Kellens K, Dewulf W, Duflou J (2015) Environmental modelling of aluminium recycling: a Life Cycle Assessment tool for sustainable metal management. J Clean Prod 105:357-370. https://doi.org/10.1016/j.jclepro.2014.09.102

Rawlings J, Pantula S, Dickey D (1998) Applied regression analysis: A research tool. Springer, New York. https://doi.org/10.1007/b98890

Richardson K, Steffen W, Lucht W, Bendtsen J, Cornell SE, Donges JF et al. (2023) Earth beyond six of nine planetary boundaries. Sci Adv 9(37):2458. https://doi.org/10.1126/sciadv.adh2458

Santarius T, Bieser JC, Frick V, Höjer M, Gossen M, Hilty LM et al. (2022) Digital sufficiency: conceptual Considerations for ICTs on a finite planet. Ann Telecommun 78(5):277-295. https://doi.org/10.1007/s12243-022-00914-x

Scarlat N, Prussi M, Padella M (2022) Quantification of the carbon intensity of electricity produced and used in Europe. Appl Energ 305:117901. https://doi.org/10.1016/j.apenergy.2021.117901

Scharnhorst W, Althaus HJ, Classen M, Jolliet O, Hilty LM (2005) The end of life treatment of second generation mobile phone networks: Strategies to reduce the environmental impact. Environ Impact Asses 25(5):540-566. https://doi.org/10.1016/j.eiar.2005.04.005

Scharnhorst W, Hilty LM, Jolliet O (2006a) Life cycle assessment of second generation (2G) and third generation (3G) mobile phone networks. Environ Int 32(5):656-675. https://doi.org/10.1016/j.envint.2006.03.001

Scharnhorst W, Althaus HJ, Hilty L, Jolliet O (2006b) Environmental assessment of end-of-life treatment options for a GSM 900 antenna rack. Int J Life Cycle Ass 11:425-436. https://doi.org/10.1065/lca2005.08.216

Scharnhorst W (2008) Life cycle assessment in the telecommunication industry: A review. Int J Life Cycle Ass 13:75-86. https://doi.org/10.1065/lca2006.11.285

Stobbe L, Richter N, Quaeck M, Knüfermann K, Druschke J, Fahland M et al. (2023) Umweltbezogene technikfolgenabschätzung mobilfunk in Deutschland – Projekt: UTAMO. Umweltbundesamt. https://www.umweltbundesamt.de/sites/default/files/medien/479/publikationen/texte_26-2023_umweltbezogene_technikfolgenabschaetzung_mobilfunk_in_deutschland.pdf. Accessed 15 October 2024

Tahseen HU, Mescia L, Catarinucci L (2023) A survey of five generations of MIMO multiband base station antennas. Radio Sci 58(7):e2023RS007725. https://doi.org/10.1029/2023RS007725

Tao J, Yu S (2015). Review on feasible recycling pathways and technologies of solar photovoltaic modules. Sol Energy Mater Sol Cells 141:108-124. https://doi.org/10.1016/j.solmat.2015.05.005

Tombaz S, Vastberg A, Zander J (2011) Energy-and cost-efficient ultra-high-capacity wireless access. IEEE Wirel Commun 18(5):18-24. https://doi.org/10.1109/MWC.2011.6056688

Wang W, Liu D, Zhang Y, Gong C (2017) Energy estimation and optimization platform for 4G and the future base station system early-stage design. China Commun 14(4):47-64. https://doi.org/10.1109/CC.2017.7927576

Wernet G, Bauer C, Steubing B, Reinhard J, Moreno-Ruiz E, Weidema B (2016) The ecoinvent database version 3 (part I): Overview and methodology. Int J Life Cycle Ass 21:1218-1230. https://doi.org/10.1007/s11367-016-1087-8

Yeung HWC (2022) Interconnected worlds: Global electronics and production networks in East Asia. Stanford University Press, California